

A comparative study of two-phase equilibria modeling tools: MORB equilibrium states at variable pressure and H₂O concentrations

DAVID HERNÁNDEZ-URIBE^{1,2,*}, FRANK J. SPERA³, WENDY A. BOHRSON⁴, AND JUSSI S. HEINONEN⁵

¹Department of Earth and Environmental Sciences, University of Michigan, Ann Arbor, Michigan 48109, U.S.A.

²Department of Earth and Environmental Sciences, University of Illinois, Chicago, Illinois 60607, U.S.A.

³Department of Earth Science and Earth Research Institute, University of California, Santa Barbara, California 93106, U.S.A.

⁴Department of Geology and Geological Engineering, Colorado School of Mines, Golden, Colorado 80401, U.S.A.

⁵Department of Geosciences and Geography, University of Helsinki, Helsinki 00014, Finland

ABSTRACT

Phase equilibria modeling is a powerful petrological tool to address both forward and inverse geological problems over a broad range of crustal and upper mantle conditions of pressure (P), temperature (T), composition (X), and redox (f_{O_2}). The development of thermodynamic databases, relatively realistic activity–composition ($a-X$) relations for solids, melts and fluids, pressure-volume-temperature (PVT) equations of state (EOS), and efficient numerical algorithms represent an inflection point in our ability to understand the nexus between tectonics and petrogenesis. While developed—and typically applied in isolation—by either metamorphic or igneous petrologists, some of the published thermodynamic models have overlapping P - T - X calibration ranges, which enables comparisons of model outcomes for similar conditions within the range of applicability. In this paper, we systematically compare the results of two such models that are routinely used for calculating phase equilibria in melt-bearing systems: rhyolite-MELTS (Gualda et al. 2012; Ghiorso and Gualda 2015) and the metabasite set of Green et al. (2016) using the thermodynamic database ds62 (Holland and Powell 2011) (hereafter denoted as “HPx-mb16”). We selected a N-MORB composition and modeled closed system equilibrium phase relations as a function of temperature at 0.25 and 1 GPa for N-MORB with 0.5 and 4 wt% H₂O. Our results show that phase relations exhibit some key differences that, in some instances, impact geological inferences. For example, clinopyroxene and plagioclase stabilities are expanded to higher temperatures in HPx-mb16 compared to predictions from rhyolite-MELTS. Orthopyroxene and olivine are stable in greater proportions and at wider temperature ranges in rhyolite-MELTS compared to HPx-mb16. Importantly, HPx-mb16 predicts amphibole in all runs presented here, whereas amphibole is only predicted at high- P -high-H₂O (1 GPa and 4 wt% H₂O) in rhyolite-MELTS, and in lesser amounts. Garnet stability is systematically expanded at higher temperatures, and the proportion is greater in rhyolite-MELTS. In addition to phase assemblage differences, phase compositions may differ. For example, plagioclase anorthite content is systematically higher in HPx-mb16 (for the same set of conditions), whereas garnet Mg# is higher in rhyolite-MELTS. Calculated amphibole compositions are substantially different between the two models as well. Liquid compositions also show important differences. High- T liquids are generally similar in SiO₂ contents but diverge at lower temperatures; in these cases, HPx-mb16 liquids are SiO₂-depleted compared to those produced by rhyolite-MELTS. Liquids are also systematically and substantially more mafic in HPx-mb16, and alumina and the alkali concentrations are relatively different and show different trends as a function of temperature at constant pressure. Overall, liquid compositions show the greatest differences near the solidus. Differences in modal abundances of phases and liquid compositions influence liquid trace-element signatures, and these differences can affect geological interpretations. Finally, a comparison between melting experiments of basaltic bulk composition and both thermodynamic models shows that rhyolite-MELTS better reproduces the higher temperature experiments, whereas HPx-mb16 better reproduces the lower temperature experiments. We discuss these and other similarities and differences to highlight the strengths and limitations of each model and to recognize that modeling results have important implications for interpretations of geologic processes. We recognize that our results are informed by a small subset of calculations over a limited range of conditions—but encourage further comparisons over a wider range of conditions and compositions.

Keywords: Phase equilibria modeling, computational petrology, rhyolite-MELTS, Theriak-Domino, thermodynamics

INTRODUCTION

The use of thermodynamics to comprehensively model multiphase and multicomponent igneous and metamorphic systems

is one of the most important developments in the Earth Sciences of the past several decades (Ghiorso and Sack 1995; Powell et al. 1998). Phase equilibria modeling can predict equilibrium phase relationships over a wide range of pressure and temperature conditions (P - T) for a variety of bulk compositions under various

* E-mail: dav.hernandez.uribe@gmail.com. Orcid 0000-0002-5335-4131

redox conditions (Powell et al. 1998, 2005; Powell and Holland 2008; Gualda et al. 2012). While there are inherent limitations associated with the use of any phase equilibria model—including the neglect of reaction kinetics, solid and liquid state diffusion, spatial P - T gradients, and uncertainties associated with thermodynamic properties of relevant substances—its utility in reproducing first-order observations of key Earth processes is evident (see, e.g., seminal work of Bowen 1928, 1945; Thompson 1967; Carmichael et al. 1974). Successes include phase equilibria modeling that has described magmatic systems and metamorphism in a host of environments including volcanic arcs, subduction zones, orogenic terranes, and large igneous provinces (e.g., Kerrick and Connolly 2001; White and Powell 2002; Johnson et al. 2008; Fowler and Spera 2010; Bohrsen et al. 2014; Yakymchuk and Brown 2014; García-Arias and Stevens 2017; Palin et al. 2017; Hernández-Uribe and Palin 2019; Heinonen et al. 2019; among many others).

Crystallization and partial melting are crucial for understanding heat advection and matter exchange between the mantle and the crust as the formation, extraction, ascent, and crystallization of magma is a primary mechanism that leads to differentiation on Earth and other planetary bodies (England and Thompson 1986; Brown 2007). Accurate phase equilibria predictions (of liquid-bearing systems) are thus key components of the earth scientist's toolbox to understand crucial geological processes. Multiphase and multicomponent thermodynamic modeling of partially or totally molten systems has been possible since the 1980s and the pioneering efforts have been greatly extended and improved over the past thirty years (Berman 1988; Essene 1989; Holland and Powell 1998, 2011; Ghiorso and Sack 1995; Ghiorso 2004). Standard state thermodynamic data, volatile species pressure-volume-temperature (PVT) data, and activity-composition (a - X) relations for crystalline and liquid solutions (collectively referred hereafter as “the thermodynamic model”) commonly used in igneous petrology include those in the MELTS package [rhyolite-MELTS, pMELTS, and pHMELTS calibrations (Ghiorso and Sack 1995; Asimow and Ghiorso 1998; Ghiorso et al. 2002; Asimow et al. 2004; Gualda et al. 2012; Ghiorso and Gualda 2015)]. The thermodynamic model commonly used in metamorphic petrology is mostly based on the work of Powell and Holland (1988) and Holland and Powell (1998, 2011), although there are other examples (cf. Lanari and Duesterhoeft 2019). For metamorphic systems, modeling of granitic liquid compositions is possible with the White et al. (2014) silicate liquid a - X relations based on previous liquid relations (Holland and Powell 1998, 2001; White et al. 2001, 2007), whereas basaltic melting can be modeled with the a - X relations of Jennings and Holland (2015) and Green et al. (2016). Updated a - X relations that allow modeling of melt-bearing equilibria in ultramafic-to-felsic metamorphic systems were recently published by Holland et al. (2018) and Tomlinson and Holland (2021). We emphasize that although different thermodynamic models are preferred by igneous and metamorphic petrologists, the models have overlapping calibration ranges and are used for exactly the same purpose—modeling phase equilibria and compositions in liquid-bearing silicate systems. At equilibrium closed-system conditions, partial melting of a metabasic lithology and crystallization of a basaltic liquid

exhibit identical phase relations at a given P - T state point.

Despite the common use of phase equilibria modeling in petrology, to the best of our knowledge, there have not been systematic studies to examine differences among thermodynamic models where calibrations overlap. While the study of Jennings and Holland (2015) and Holland et al. (2018) do compare their a - X relations to results from pMELTS, the focus of those papers was not a systematic comparison of the predicted equilibria. Existing comparative studies in metamorphic petrology explore the differences between the various Holland and Powell thermodynamic databases (e.g., Korhonen et al. 2014; Guevara and Caddick 2016; Pan et al. 2020; Starr et al. 2020); and compare model predictions with experiments and natural samples (e.g., White et al. 2011; Forshaw et al. 2019; Santos et al. 2019; García-Arias 2020; Bartoli and Carvalho 2021; Gervais and Trapy 2021). The MELTS package collection has also been compared to results of other thermobarometric methods on natural samples (e.g., Pamukcu et al. 2015), experimental studies not included in the model calibrations (e.g., Hirschmann et al. 1998; Neave et al. 2019; Pichavant et al. 2019), and between different MELTS calibrations (e.g., Balta and McSween 2013).

In this study, we take a combined approach. We systematically compare phase equilibria calculated with rhyolite-MELTS (Ghiorso et al. 2012; Ghiorso and Gualda 2015) and the “metabasite set” of Green et al. (2016) [“HPx-mb16,” calculated using Theriak-Domino (de Capitani and Brown 1987; de Capitani and Petrakakis 2010)] for the equilibrium states of a mid-ocean ridge basalt (MORB) at different P - T conditions and different initial H_2O contents from near-liquidus to solidus temperatures along the fayalite-magnetite-quartz (FMQ) oxygen buffer. These two thermodynamic approaches (i.e., rhyolite MELTS and HPx-mb16) are the most commonly used by igneous and metamorphic petrologists, respectively, to describe liquid-bearing mafic systems. We also evaluate how closely the calculated MORB phase equilibria between rhyolite-MELTS and HPx-mb16 compare with independent relevant experiments (i.e., not used in the calibration). We discuss the implications of our results within the framework of trace-element modeling and examine the geologic implications of the differences in model outcomes. By comparing the effects of pressure and H_2O concentration on the phase equilibria during equilibrium melting and crystallization of a MORB using two extant thermodynamic models, we provide our perspective on model uncertainty associated with the choice of modeling. The critical insight of our work is to recognize the strengths of the thermodynamic models, and to highlight similarities and differences to illustrate how the choice of thermodynamic models can lead to different geologic interpretations.

THERMODYNAMIC MODELS

Phase equilibria modeling relies on standard state thermodynamic data, the EOS and a - X relations for solid and liquid solutions. A thermodynamic database includes standard state properties for all phases, the form and numerical values defining PVT , and isobaric heat capacity expressions for all phases (Berman 1988; Essene 1989; Holland and Powell 1998, 2011; Ghiorso and Sack 1995; Ghiorso 2004). These parameters are obtained from experimental, calorimetric, and other studies (e.g.,

spectroscopy), and some are statistically treated to obtain the best-fit value for the desired parameter from multiple experiments (e.g., least-squares regressions used by Holland and Powell databases). To be “internally consistent,” all thermodynamic parameters must be compatible with thermodynamic definitions and identities, adhere to a set of reference values, consider all the experimental data simultaneously, and reproduce primary data within their uncertainties (Lanari and Duesterhoeft 2019 and references therein). The rhyolite-MELTS thermodynamic database is based on Berman (1988) with modifications (see Ghiorso and Sack 1995; Asimow and Ghiorso 1998; Gualda et al. 2012; Ghiorso and Gualda 2015 for details). The thermodynamic data used in HPx-mb16 utilizes version 6.2 of Holland and Powell (2011). Some important differences between these thermodynamic data include—but are not limited to—how the equations of state of the solid phases are calculated (i.e., using the Tait equation of state in Holland and Powell (2011) vs. the EOS modified from Berman (1988) in the MELTS package) and the isobaric 1-bar heat capacity dependence on temperature (i.e., the Robie et al. (1978) equation in Holland and Powell (2011) vs. the high- T form used in the Berman and Brown (1985) equation for the MELTS package). Furthermore, the PVT properties of fluid utilized in the MELTS package are calculated using the model of Ghiorso and Gualda (2015), whereas in Holland and Powell (2011) the equation of state of Pitzer and Sterner (1995) is used. For a comprehensive review of all the parameters used in these two thermodynamic models, the reader is referred to the original references.

In addition to standard state thermodynamic properties for pure phases, one must also treat the non-ideal properties of crystalline, liquid, and gaseous solutions. The excess Gibbs energies of multicomponent solutions are handled using a - X relations that relate Gibbs excess energies as a function of pressure, temperature, and solution composition to activity coefficients. The solid-solution models describe the thermodynamics of mixing between end-members of the multicomponent solution and reflect the elemental substitutions that take place in crystalline solids, including ordering and exsolution. The a - X relations for solid-solution phases commonly contain end-member proportions, crystallographic site fractions, mixing parameters (also known as the Margules parameter), ideal parameters, and thermodynamic adjustments (Lanari and Duesterhoeft 2019 and references therein). Mixing relationships can be ideal, symmetrical, or asymmetrical, depending on the behavior of the Margules parameter pair. The excess Gibbs energy is normally a function of temperature and pressure. We mention the a - X relations (and the elements considered) that were used in this work in the next section, and other details are given in the Online Materials¹ Table S1.

One approach to calculating phase equilibria is by solving simultaneous non-linear equations to build up an array of points and lines that make up the phase diagram by using Schreinemakers' analysis (e.g., THERMOCALC; Powell et al. 1998), whereas another approach is Gibbs free energy minimization to determine the most stable phase assemblage at specific state points. This second approach is used in the MELTS package (Ghiorso and Sack 1995; Asimow and Ghiorso 1998; Gualda et al. 2012; Ghiorso and Gualda 2015) and in Theriak-Domino and `Perple_X` (Connolly 2005; de Capitani and Petrakakis 2010).

PETROLOGICAL MODELING

Modeling setups

Phase equilibria calculations for this study were performed using rhyolite-MELTS and Theriak-Domino in the Na_2O - CaO - K_2O - FeO - MgO - Al_2O_3 - SiO_2 - H_2O - TiO_2O_2 (NCKFMASHTO) system. This system was chosen because the HPx-mb16 model was calibrated in this 10-component system (Green et al. 2016), which is also appropriate for rhyolite-MELTS.

For the rhyolite-MELTS runs, we used the internally consistent thermodynamic database of Berman (1988) with some modifications (Gualda et al. 2012; Ghiorso and Gualda 2015) and the a - X relations for solid-solution phases included in the rhyolite-MELTS calibration (Online Materials¹ Table S1), i.e., silicate liquid (Ghiorso and Sack 1995); pyroxene (Sack and Ghiorso 1994); orthopyroxene, biotite, olivine (Sack and Ghiorso 1989); amphibole (Ghiorso et al. 1995); garnet (Berman 1990; Berman and Koziol 1991); feldspar (Elkins and Grove, 1990); spinel (Sack and Ghiorso 1991a, 1991b); and rhombohedral oxide (Ghiorso 1990; Ghiorso and Sack 1991; Ghiorso and Evans 2008). Note that, despite its name, rhyolite-MELTS is meant for modeling mafic systems and the prefix “rhyolite” only refers to the latest calibration that is more suitable also for felsic systems than the preceding MELTS versions (Gualda et al. 2012; <http://melts.ofm-research.org>).

For the Theriak-Domino runs, we utilized the Theriak-Domino version from D.K. Tinkham (<https://dtinkham.net/peq.html>), the internally consistent thermodynamic database ds62 (Holland and Powell 2011), and the “metabasite set” of a - X relations for solution phases (Online Materials¹ Table S1) from Green et al. (2016); these include: liquid, augite and clinopyroxene (Green et al. 2016); garnet, biotite, chloritoid, muscovite-paragonite, and chlorite (White et al. 2014); epidote (Holland and Powell 2011); plagioclase (Holland and Powell 2003); magnetite-spinel (White et al. 2002); and ilmenite-hematite (White et al. 2000). Pure phases include albite, quartz, rutile, and titanite.

In all comparative calculations in this study, we computed equilibrium state points only; fractionation was not used except as a preliminary step in rhyolite-MELTS to determine the appropriate version of rhyolite-MELTS. Hence our calculations apply equally to equilibrium crystallization and to equilibrium partial melting as these processes are thermodynamically identical.

The wide P - T - X ranges of the modeling software enable near-infinite possibilities for model comparison. Here, we focus on a detailed comparison of one of the most widely used average compositions in petrological modeling, that of the mean N-MORB from Gale et al. (2013) (Table 1). Modeling intermediate and/or felsic systems is outside of the scope of this study. To explore the effects of H_2O in our calculation, we utilized two initial H_2O contents: 0.5 and 4 wt%, to account for relatively dry and wet conditions. The oxygen chemical potential was controlled by imposing the FMQ buffer in all calculations.

Calculations were carried out at 0.25 and 1 GPa, which approximate upper and lower crustal conditions, and were calculated isobarically over the temperature interval between 600 °C to the liquidus temperature (calculated by rhyolite-MELTS) in discrete steps. In rhyolite-MELTS, the FMQ buffer is not maintained below the solidus, and thus, results below such conditions are not discussed in this study.

TABLE 1. Bulk-rock compositions used for petrological modeling (normalized wt%)

	N-MORB-0.5	N-MORB-4
SiO ₂	50.69	48.91
TiO ₂	1.54	1.48
Al ₂ O ₃	15.21	14.68
FeO ⁱ	9.86	9.52
MgO	7.80	7.53
CaO	11.41	11.01
Na ₂ O	2.85	2.75
K ₂ O	0.14	0.14
H ₂ O	0.50	4.00
Total	100.00	100.00

Note: All compositions correspond to the mean N-MORB from Gale et al. (2013) but with different H₂O contents.

Comparison methodology

We performed a comparison using four sets of conditions. These include: (1) a low-*P*-low-H₂O run (i.e., at 0.25 GPa and 0.5 wt% H₂O); (2) a low-*P*-high-H₂O run (i.e., at 0.25 GPa and 4 wt% H₂O); (3) a high-*P*-low-H₂O run (i.e., at 1 GPa and 0.5 wt% H₂O); and (4) a high-*P*-high-H₂O run (i.e., at 1 GPa and 4 wt% H₂O). All calculations were carried out at discrete temperatures spanning the solidus to liquidus (or near-liquidus) temperatures along with the selected pressures. As noted earlier, the equilibrium (closed system) states computed apply to both crystallization and melting because, at equilibrium, the liquid-solid-fluid relationships are the same for closed-system melting or crystallization. Thus, we emphasize that although the calculations (and Figs. 1, 2, and 4–7) proceed from near-solidus toward liquidus temperatures (i.e., equilibrium partial melting), the calculations are equally applicable to down-temperature equilibrium crystallization since there is no fractionation of solids from liquid.

Because there are several versions of rhyolite-MELTS, we followed the decision tree on the rhyolite-MELTS website (<http://melts.ofm-research.org/LIQUIDS-decision-tree.html>) to choose the appropriate version for each calculation. All the rhyolite-MELTS runs were calculated with the version v1.2.0 with the exception of the low-*P*-high-H₂O run (i.e., at 0.25 GPa and 4 wt% H₂O), where v1.1.0 was used.

Modal phase proportions are shown using mode boxes, which include the calculated normalized mass proportions (wt%) of all predicted phases at each calculated state point (Figs. 1 and 2; mineral proportions in vol% are also shown in Online Material¹ Figures S1 and S2). When more than one phase of the same solid solution was stable at a single state point (e.g., two clinopyroxenes predicted by rhyolite-MELTS), the phase masses were combined for simplicity. Calculated modal proportions are given in Table 2 every 100 °C from 900 (or 800 °C) to 1100 °C. A detailed description of the calculated phase equilibria evolution for the four scenarios is given in Online Materials¹ Appendix 1.

Liquid compositions are reported from the liquidus (calculated with rhyolite-MELTS) or near liquidus (HPx-mb16) to the solidus (Figs. 3–7). Given that the rhyolite-MELTS liquid *a-X* model, in contrast to the Green et al. (2016) liquid *a-X* model, considers both FeO and Fe₂O₃, the Fe content of the calculated compositions was recalculated to FeOⁱ allowing for direct comparison. Liquid compositions are given in Online Materials¹ Tables S2 and S3 every 100 °C from 900 (or 800 °C) to 1100 °C. Compositions are reported in the table only when liquid is stable in both rhyolite-MELTS and HPx-mb16 models at the same *P-T* conditions. The full liquid compositional evolution is described in Online Materials¹ Appendix 1.

In addition to providing a first-order comparison of the phase relations and liquid compositions, we also compare composi-

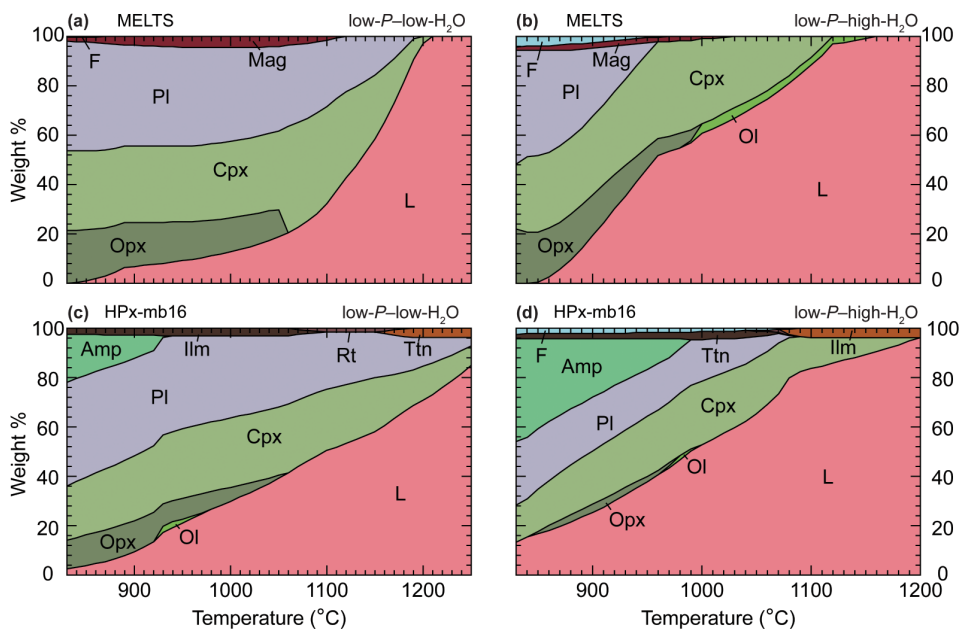


FIGURE 1. Equilibrium phase assemblages at 0.25 GPa for a N-MORB composition. (a and b) rhyolite-MELTS and (c and d) HPx-mb16. (a, c) Low-H₂O (0.5 wt% H₂O) calculations. (b and d) High-H₂O (4 wt% H₂O) calculations. Mineral abbreviations follow Whitney and Evans (2010) with the exception of “L” and “F” which refer to liquid and fluid, respectively. (Color online.)

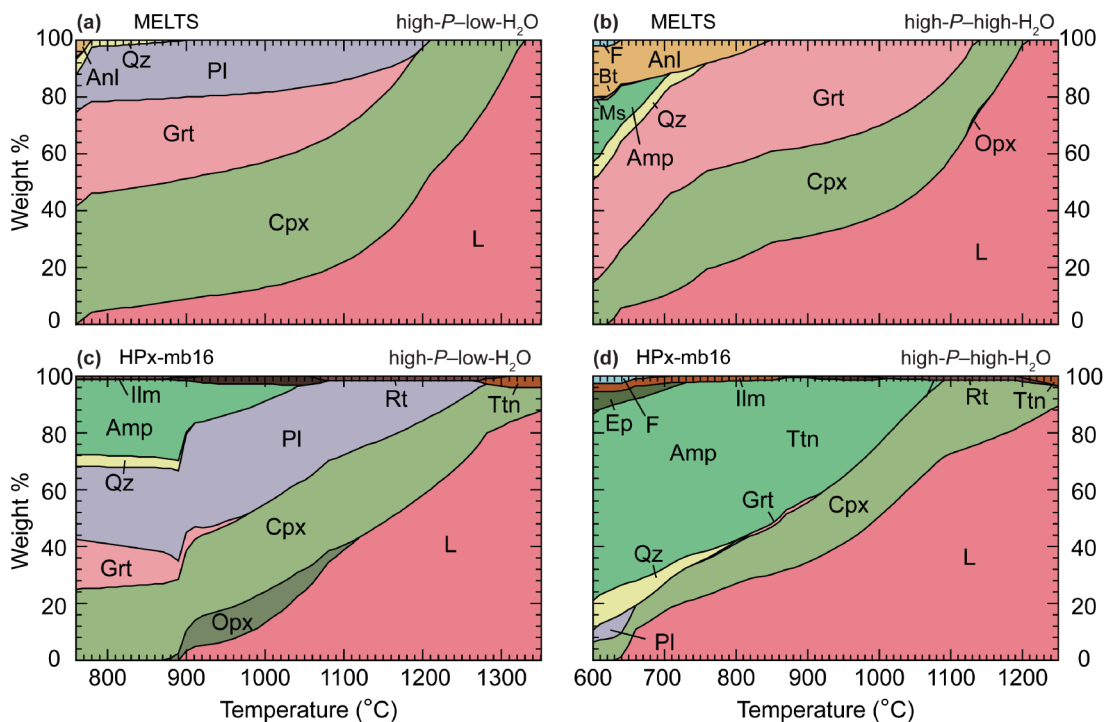


FIGURE 2. Equilibrium phase assemblages at 1 GPa for a N-MORB composition. (a and b) rhyolite-MELTS and (c and d) HPx-mb16. (a and c) Low- H_2O (0.5 wt% H_2O) calculations. (b and d) High- H_2O (4 wt% H_2O) calculations. Mineral abbreviations follow Whitney and Evans (2010) with the exception of “L” and “F” which refer to liquid and fluid, respectively. (Color online.)

tions of clinopyroxene, feldspar, orthopyroxene, amphibole, and garnet, which are the most abundant minerals. A detailed description of the phase compositions at each state point can be found in the Online Materials¹ Appendix 1 and in Online Material¹ Figures S3–S6. Only the most significant mineral-compositional differences and characteristics are presented and discussed in the sections below.

Models caveats

Both of the thermodynamic models used here (i.e., rhyolite-MELTS and HPx-mb16) have significant caveats, limitations, and uncertainties, mainly related to the thermodynamic data and the $a-X$ models. A detailed discussion is beyond the scope of this paper; the reader is referred to the original works and developers’ websites to find important information related to the models (rhyolite-MELTS, <http://melts.ofm-research.org>; HPx-mb16, <https://hpxeosandthermocalc.org>). Below, we only outline the calibration ranges where the thermodynamic models should yield reliable results and some important caveats pertinent to our comparison work.

Rhyolite-MELTS is recommended for modeling relatively dry mafic and hydrous silicic systems at <2 GPa. Phase equilibria calculations via rhyolite-MELTS are not recommended at conditions close to the solidus (and subsolidus) and/or for intermediate and calc-alkaline systems with modally significant amphibole, muscovite, and biotite (<http://melts.ofm-research.org>; Gualda et al. 2012). Rhyolite-MELTS calculations are further recommended for volcanic systems where the melt fraction is >50 wt% (Gualda et al. 2012).

Calculations with the HPx-mb16 model are recommended for modeling partial melting of hydrous metabasites at <1.3 GPa. Reliable phase equilibria can be calculated at subsolidus and suprasolidus conditions up to ~ 1050 °C (Green et al. 2016; Palin et al. 2016); yet, modeling phase equilibria near- or at the liquidus is not recommended as the liquid $a-X$ model accounts for neither Fe_2O_3 and TiO_2 .

MODEL COMPARISON

Differences in the calculated phase proportions

Overall, rhyolite-MELTS calculates more liquid at higher temperatures (closer to the liquidus) but less liquid at lower temperatures (closer to the solidus) compared to HPx-mb16 (Figs. 1 and 2). For example, in the low- P -low- H_2O run at 1100 °C, rhyolite-MELTS predicts ~ 33 wt% liquid, whereas HPx-mb16 predicts ~ 50 wt% liquid (~ 36 and ~ 53 vol%, respectively; Figs. 1a and 1c; Online Materials¹ Figs. S1a and S1c; Table 2). The position of the solidi varies depending on pressure between the two models as well. In the low- P runs, the solidus is located at higher temperature (e.g., ~ 850 vs. ~ 730 °C in the high- H_2O run; Figs. 1b and 1d), whereas in the high- P run, it is located at lower temperature (e.g., ~ 760 vs. ~ 890 °C in the low- H_2O run; Figs. 2a and 2c) in rhyolite-MELTS compared to HPx-mb16. In all the calculations, a higher H_2O content decreases the solidus temperature (Figs. 1 and 2).

Clinopyroxene and plagioclase stabilities are expanded to higher temperatures in HPx-mb16 regardless of the conditions (Figs. 1 and 2). At temperatures closer to the solidus, rhyolite-

TABLE 2a. Phase proportions of N-MORB at 0.25 GPa (wt%)

	0.25 GPa, 0.5 wt% H ₂ O						0.25 GPa, 4 wt% H ₂ O					
	900 °C		1000 °C		1100 °C		900 °C		1000 °C		1100 °C	
	MELTS	HPx-mb16	MELTS	HPx-mb16	MELTS	HPx-mb16	MELTS	HPx-mb16	MELTS	HPx-mb16	MELTS	HPx-mb16
L	7	9	13	30	32	50	19	26	61	52	88	84
Ol	–	–	–	–	–	–	–	–	4	1	3	–
Opx	18	13	14	6	–	–	17	3	–	–	–	–
Cpx	31	26	31	28	39	25	32	21	34	25	8	13
Fsp	41	40	38	33	27	23	27	22	–	17	–	–
Amp	–	9	–	–	–	–	–	24	–	–	–	–
Ilm	–	3	–	3	–	–	–	2	–	3	–	–
Mag	4	–	5	–	2	–	2	–	1	–	–	–
Rt	–	–	–	–	–	2	–	–	–	–	–	4
F	–	–	–	–	–	–	2	2	–	1	–	<1
Total	100	100	100	100	100	100	100	100	100	100	100	100

Note: Mineral abbreviations follow Whitney and Evans (2010) with the exception of "L" and "F" which refer to liquid and fluid, respectively.

TABLE 2b. Phase proportions of N-MORB at 1 GPa (wt%)

	1 GPa, 0.5 wt% H ₂ O						1 GPa, 4 wt% H ₂ O									
	800 °C		900 °C		1000 °C		800 °C		900 °C		1000 °C		1100 °C			
	MELTS	HPx-mb16	MELTS	HPx-mb16	MELTS	HPx-mb16	MELTS	HPx-mb16	MELTS	HPx-mb16	MELTS	HPx-mb16	MELTS	HPx-mb16		
L	5	0	9	3	13	13	22	39	23	27	31	34	38	50	59	73
Opx	–	–	–	7	–	11	–	2	–	–	–	–	–	–	–	–
Cpx	42	26	42	28	44	31	47	32	34	14	32	21	32	26	29	26
Grt	32	15	29	7	25	–	17	–	38	–	37	1	30	–	12	–
Fsp	19	27	20	35	18	36	14	26	–	1	–	–	–	–	–	–
Qz	2	4	<1	1	–	–	–	–	–	<1	–	–	–	–	–	–
Amp	–	27	–	18	–	6	–	–	–	56	–	43	–	23	–	–
Anl	–	–	–	–	–	–	–	–	5	–	–	–	–	–	–	–
Ilm	–	–	–	1	–	3	–	–	–	–	–	<1	–	1	–	–
Ttn	–	–	–	–	–	–	–	–	–	–	–	1	–	1	–	1
Rt	–	1	–	1	–	–	–	2	–	2	–	–	–	–	–	–
Total	100	100	100	100	100	100	100	100	100	100	100	100	100	100	100	100

Note: Mineral abbreviations follow Whitney and Evans (2010) with the exception of "L" and "F" which refer to liquid and fluid, respectively.

MELTS predicts higher amounts of these phases, and the specific temperatures where rhyolite-MELTS predicts more of these phases depend on the specific run (Figs. 1 and 2; Table 2). For example, in the low-*P*–high-*H*₂O run at 900 °C, rhyolite-MELTS predicts ~32 wt% of clinopyroxene and ~27 wt% of plagioclase (~24 and ~26 vol%, respectively), whereas HPx-mb16 predicts ~21 wt% clinopyroxene and ~22 wt% plagioclase (~16 and ~21 vol%, respectively) (Figs. 1b and 1d; Online Materials¹ Figs. S1b and S1d; Table 2). Plagioclase proportion is systematically higher in rhyolite-MELTS at any given temperature in the low-*P* runs. For example, at 830 °C in the low-*P*–high-*H*₂O run, rhyolite-MELTS calculates ~46 wt% of plagioclase, whereas HPx-mb16 predicts ~25 wt% (~43 and ~25 vol%, respectively; Figs. 1b and 1d; Online Materials¹ Fig. S1b and S1d). By contrast, in the high-*P*

runs, plagioclase systematics are different; in the low-*H*₂O run, rhyolite-MELTS calculates less amount of plagioclase compared to HPx-mb16, whereas in high *H*₂O run, only HPx-mb16 predicts plagioclase (Fig. 2; Table 2).

Orthopyroxene and olivine proportions are systematically higher in the rhyolite-MELTS low-*P* runs compared to HPx-mb16 low-*P* runs (Fig. 1); olivine stability is typically expanded to higher temperatures in rhyolite-MELTS compared to HPx-mb16. In the low-*P*–low-*H*₂O run, olivine is not stable in rhyolite-MELTS but is predicted in a small temperature window in the HPx-mb16 calculation (Fig. 1). By contrast, in the high-*P* runs, orthopyroxene and olivine are not stable except orthopyroxene only in the low-*H*₂O HPx-mb16 run.

A crucial systematic difference in all *P*-*T*-*H*₂O conditions is

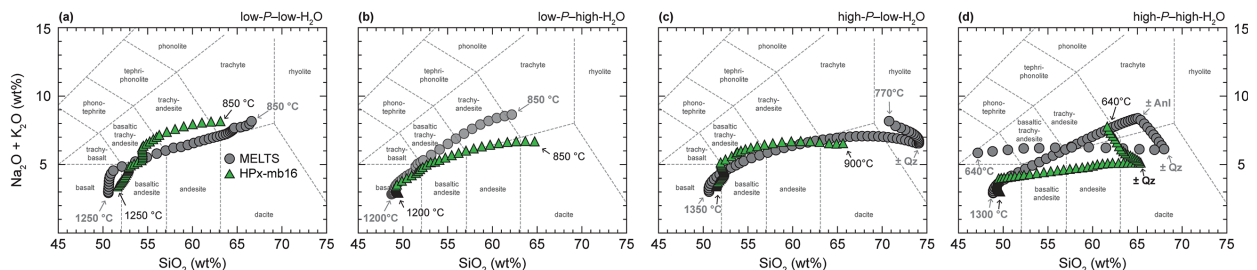


FIGURE 3. Total alkali-silica (TAS) classification diagram (Le Bas et al. 1986) for the calculated N-MORB liquids (liquid compositions correspond to those presented in Figs. 1 and 2). Liquid compositions are shown every 10 °C from the liquidus to the solidus. (Color online.)

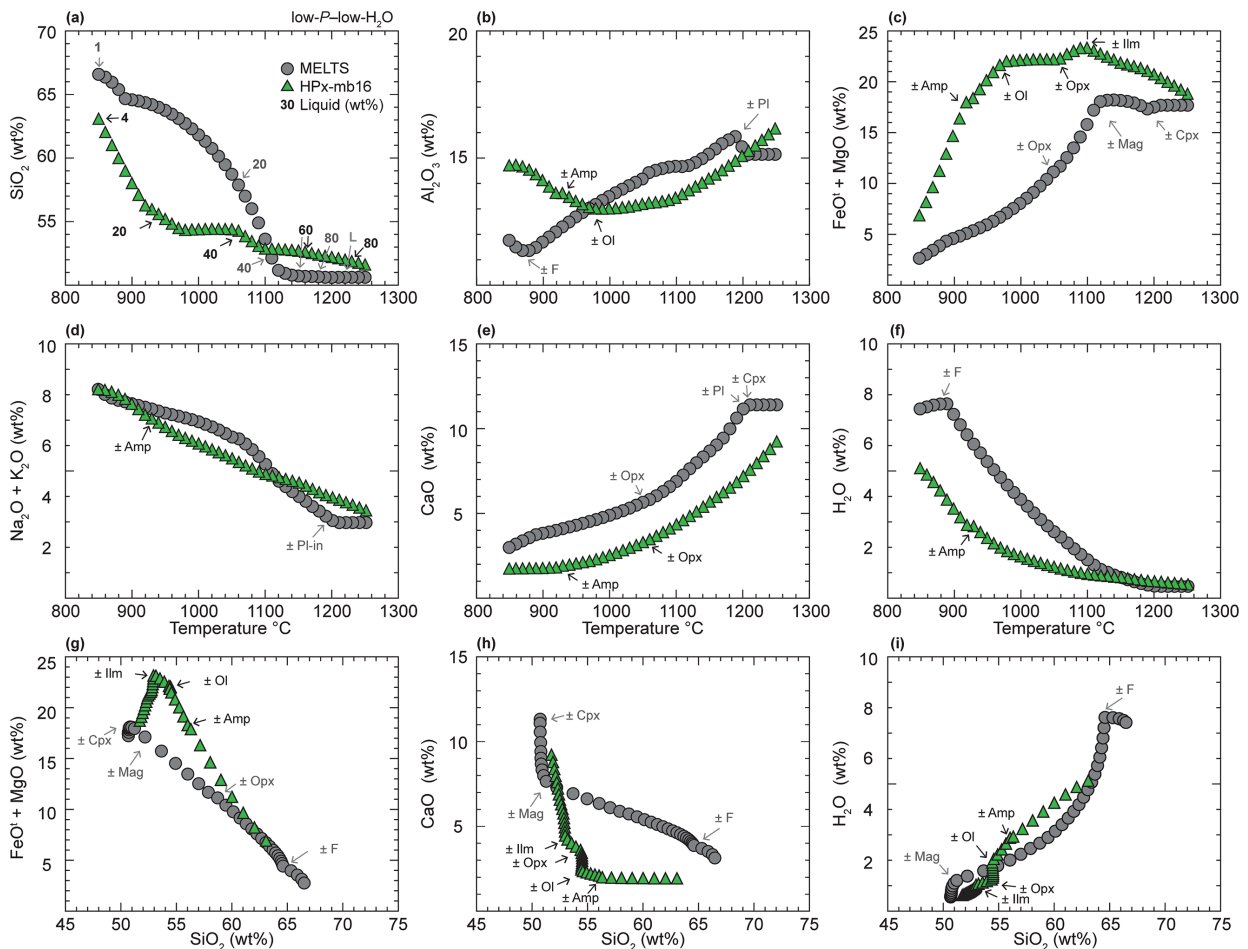


FIGURE 4. Liquid compositional evolution (wt%) at 0.25 GPa for a low- H_2O (0.5 wt% H_2O) N-MORB composition. (a–f) Calculated liquid compositions as a function of temperature. (g–i) Liquid compositions shown in Harker diagrams. Approximate liquid fractions (wt%) are shown in a for comparison between modeling approaches. Mineral abbreviations follow Whitney and Evans (2010) with the exception of “L” and “F” which refer to liquid and fluid, respectively. (Color online.)

the stability of amphibole. HPx-mb16 predicts amphibole in all runs; the amount of amphibole increases with increasing pressure and H_2O (Figs. 1c, 1d, 2c, and 2d; Table 2). By contrast, in the rhyolite-MELTS calculations, amphibole is only predicted in the high- P -high- H_2O run (Fig. 2b). The amount of amphibole, and its temperature-interval of stability, are not comparable with HPx-mb16 (Figs. 2b–2d). For example, in the high- P -high- H_2O run at 700 °C, rhyolite-MELTS predicts ~2 wt% of amphibole compared to ~63 wt% in HPx-mb16 (~1 and ~57 vol%, respectively; Figs. 2b and 2d; Online Materials¹ Fig. S2b and S2d). At 600 °C in the same run, the modal difference remains considerable: rhyolite-MELTS predicts ~22 wt% of amphibole, whereas in HPx-mb16 modal amphibole is ~66 wt% (~20 and ~61 vol%, respectively; Figs. 2b and 2d; Online Materials¹ Fig. S2b and S2d).

Garnet is only stable in the high- P runs in both models. Its stability is systematically expanded to higher temperatures, and the proportion is greater in rhyolite-MELTS compared to HPx-mb16 (Fig. 2). For instance, in the high- P -low- H_2O run at 800 °C, rhyolite-MELTS predicts ~32 wt% of garnet, whereas HPx-mb16

predicts ~15 wt% (~27 and ~12 vol%, respectively; Figs. 2a and 2c; Online Materials¹ Figs. S2a and S2c; Table 2). Unexpectedly, higher H_2O increases the proportion of garnet in rhyolite-MELTS (Figs. 2a and 2b). On the other hand, HPx-mb16 follows the opposite trend relative to H_2O (Figs. 2c and 2d), i.e., a higher H_2O inhibits garnet stabilization.

Other minor phases, such as quartz and Fe-Ti oxides, also show differences between the models (Figs. 1 and 2). Quartz is predicted at relatively similar temperatures (± 50 °C) but is systematically higher in proportion in rhyolite-MELTS in the low- H_2O runs but lower in the high- H_2O runs (Figs. 1 and 2). By contrast, proportions of Fe-Ti oxides are relatively similar (± 2 wt%), although the predicted phase is always different in the low- P runs: rhyolite-MELTS predicts a spinel group phase (ulvospinel–magnetite) whereas HPx-mb16 predicts rutile that is replaced by ilmenite at a lower temperature (Figs. 1 and 2).

The models predict H_2O -saturation conditions at different P - T conditions (Figs. 1 and 2). In the low- P -low- H_2O run, H_2O -saturated conditions are only attained in rhyolite-MELTS (Fig.

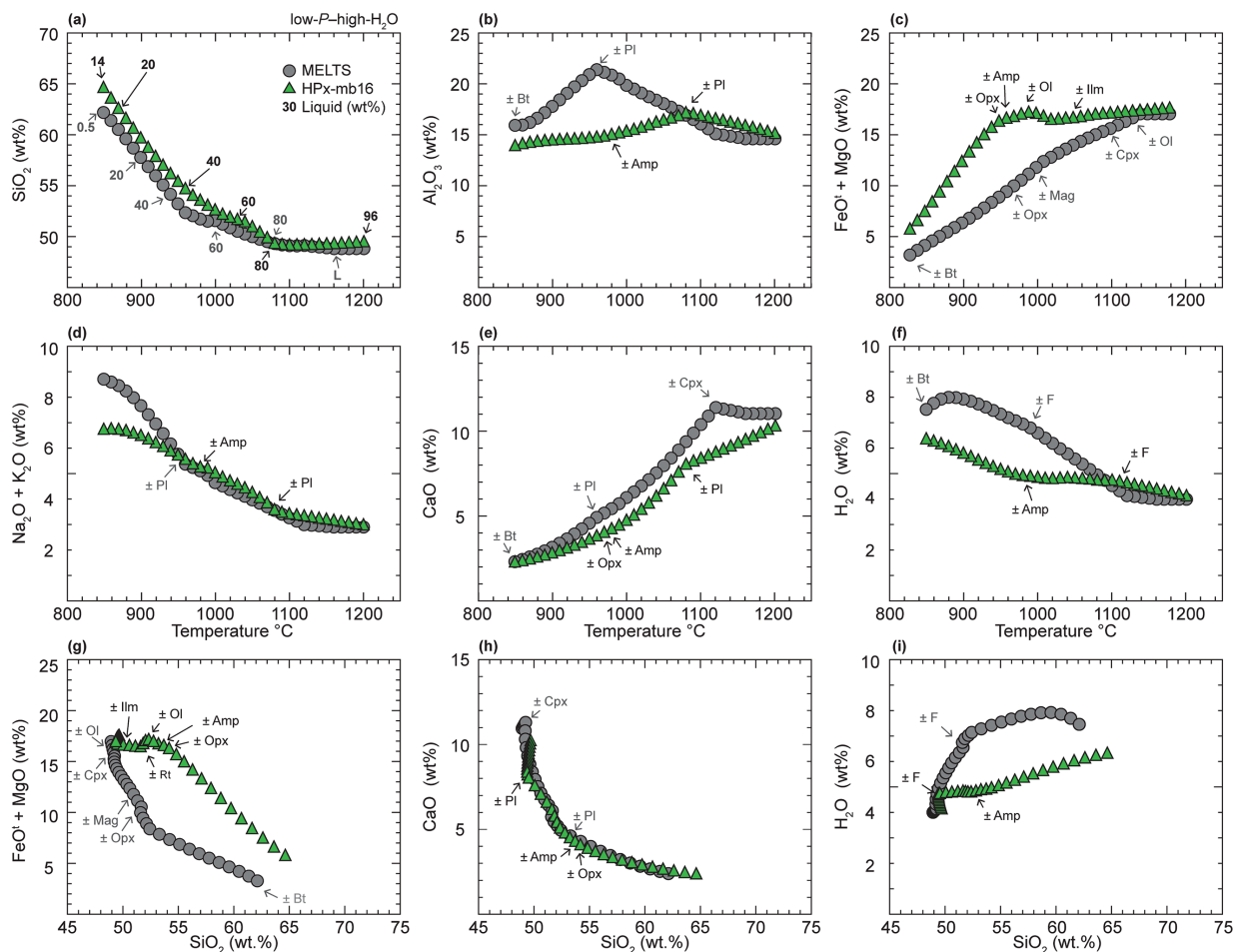


FIGURE 5. Liquid compositional evolution (wt%) at 0.25 GPa for a high-H₂O (4 wt% H₂O) N-MORB composition. (a–f) Modeled liquid compositions as a function of temperature. (g–i) Modeled liquid compositions shown in Harker diagrams. Approximate liquid fractions (wt%) are shown in **a** for comparison between modeling approaches. Mineral abbreviations follow Whitney and Evans (2010) with the exception of “L” and “F” which refer to liquid and fluid, respectively. (Color online.)

1a). By contrast, in the low-*P*–high-H₂O run, all calculations reach H₂O-saturated conditions, although H₂O as a phase occurs at higher temperatures and in lower proportion in HPx-mb16 (Figs. 1b and 1d). In the small temperature interval where the system is H₂O-saturated in HPx-mb16 but not in rhyolite-MELTS (i.e., ~1100–1000 °C; Figs. 1b and 1d), the liquid proportion is higher in rhyolite-MELTS (Figs. 1b and 1d). In the high-*P* runs, H₂O-saturated conditions are only reached in the high-H₂O run in both models (Figs. 2b and 2d). Similar to the low-*P* runs, H₂O occurs at slightly higher temperatures in HPx-mb16 runs (Figs. 2b and 2d).

In all our calculations, there are four phases that are only stable in either rhyolite-MELTS or in HPx-mb16. These are analcime (only predicted by rhyolite-MELTS) and epidote, titanite, and rutile (only predicted by HPx-mb16). (Figs. 1 and 2).

Differences in the calculated phase compositions

Liquid compositions. The calculated silicate liquids follow relatively similar compositional trends as a function of temperature (Fig. 3); changes in liquid composition are controlled by the

crystallization or consumption of phases which, as noted above, differ between models.

Generally, high-*T* liquid compositions are relatively similar in SiO₂ but, for most calculations, diverge at lower temperatures. In the low-*P*–low-H₂O run, the SiO₂ is enriched in HPx-mb16 at high temperatures compared to the liquid predicted by rhyolite-MELTS (Fig. 4a). At lower temperatures in the low-H₂O runs, HPx-mb16 liquid compositions are SiO₂-depleted compared to rhyolite-MELTS (up to ~5 wt%; Figs. 4a and 6a); by contrast, in the high-H₂O runs, the HPx-mb16 liquid compositions are SiO₂-enriched compared to rhyolite-MELTS (up to ~16 wt%; Figs. 5a and 7a). The liquid SiO₂ contents in the low-*P*–high-H₂O runs in rhyolite-MELTS and HPx-mb16 are almost identical (Fig. 5a).

Calculated liquids are systematically—and substantially—more mafic in the HPx-mb16 than in rhyolite-MELTS (up to ~18 wt% higher in the high-*P*–low-H₂O run at 1080 °C; Fig. 6c). Liquid FeO⁺ + MgO in HPx-mb16 shows a distinct enrichment at high temperatures that is not observed in rhyolite-MELTS (Figs. 4c, 5c, 6c, and 7c). These changes are less significant as

the H₂O content increases at the same pressure (Figs. 4c and 5c); the high-*P*-high-H₂O run shows the least difference in liquid FeO + MgO (Fig. 7c).

The CaO and H₂O concentrations of the melts have similar compositional trends in both models and tend to be higher in rhyolite-MELTS. The relative difference in the CaO and H₂O contents is greater in the low-*P* runs (up to 5 wt% in CaO and ~4 wt% in H₂O Figs. 4f and 5f); by contrast, in the high-*P* runs, the difference in the liquid CaO and H₂O contents is smaller (Figs. 6f and 7f). In all the runs, the H₂O liquid content tends to diverge the most at lower temperatures (Figs. 4f, 5f, 6f, and 7f).

Liquid Al₂O₃ and alkali contents are relatively different between the models throughout. The liquid Al₂O₃ contents follow different trends in all the runs (Figs. 4b, 5b, 6b, and 7b); the alkali contents are relatively similar in all the low-*P* runs (Figs. 4d and 5d). In the high-*P* runs, within 1200–900 °C (in the low-H₂O content run) and 1100–750 °C (in the high-H₂O content run), the rhyolite-MELTS calculated liquid compositions are greater in alkali contents compared to the HPx-mb16 liquid compositions (up to 2–3 wt%; Figs. 6d and 7d).

Overall, liquid compositions show the greatest difference at lower temperatures, closer to the solidus: the low-*P* runs are the most similar (especially CaO and alkalis; Figs. 4 and 5), whereas, in the high-*P* runs, compositional differences are more distinct (especially in the case of SiO₂, Al₂O₃, and H₂O; Figs. 6 and 7).

Mineral compositions. Details of the mineral chemical evolution and the results derived from both models can be found in Online Materials¹ Appendix 1 and in the Online Material¹ Figures S2–S5. Among the most important differences is that the clinopyroxene shows similar Mg# [Mg# = Mg/(Fe²⁺ + Mg)] at temperatures near the liquidus, but with decreasing temperature, rhyolite-MELTS predicts higher clinopyroxene Mg# values compared to HPx-mb16 in all runs. Plagioclase anorthite content is systematically higher in HPx-mb16 at any temperature compared to rhyolite-MELTS in all the runs. In the high-*P* runs, garnet Mg# values are systematically higher in rhyolite-MELTS compared to HPx-mb16 at any given temperature; almandine and grossular contents are systematically higher, and pyrope contents lower in HPx-mb16. Calculated amphibole compositions are substantially different between rhyolite-MELTS and HPx-mb16, reflecting the

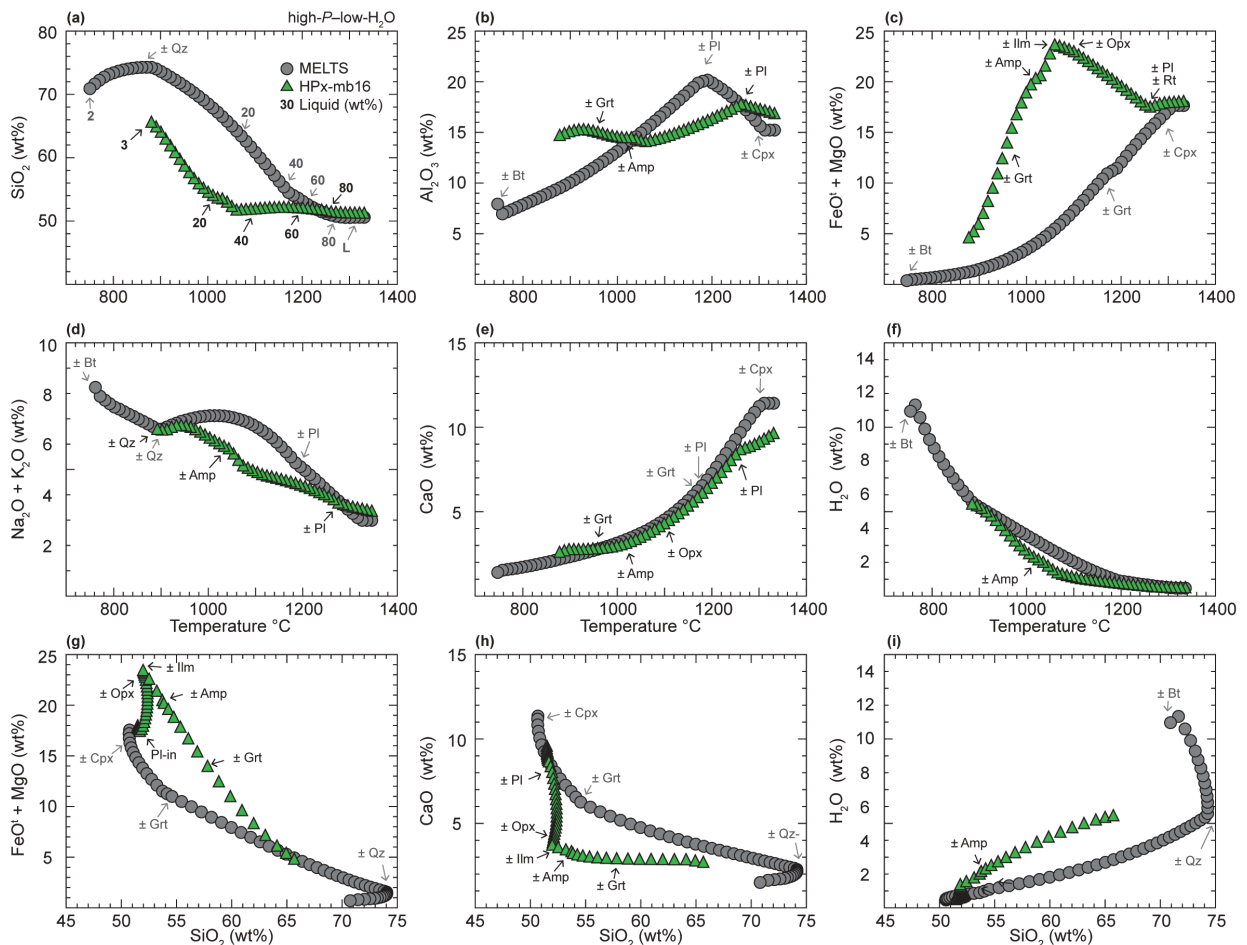


FIGURE 6. Liquid compositional evolution (wt%) at 1 GPa for a low-H₂O (0.5 wt% H₂O) N-MORB composition. (a–f) Modeled liquid compositions as a function of temperature. (g–i) Modeled liquid compositions shown in Harker diagrams. Approximate liquid fractions (wt%) are shown in a for comparison between modeling approaches. Mineral abbreviations follow Whitney and Evans (2010) with the exception of “L” and “F” which refer to liquid and fluid, respectively. (Color online.)

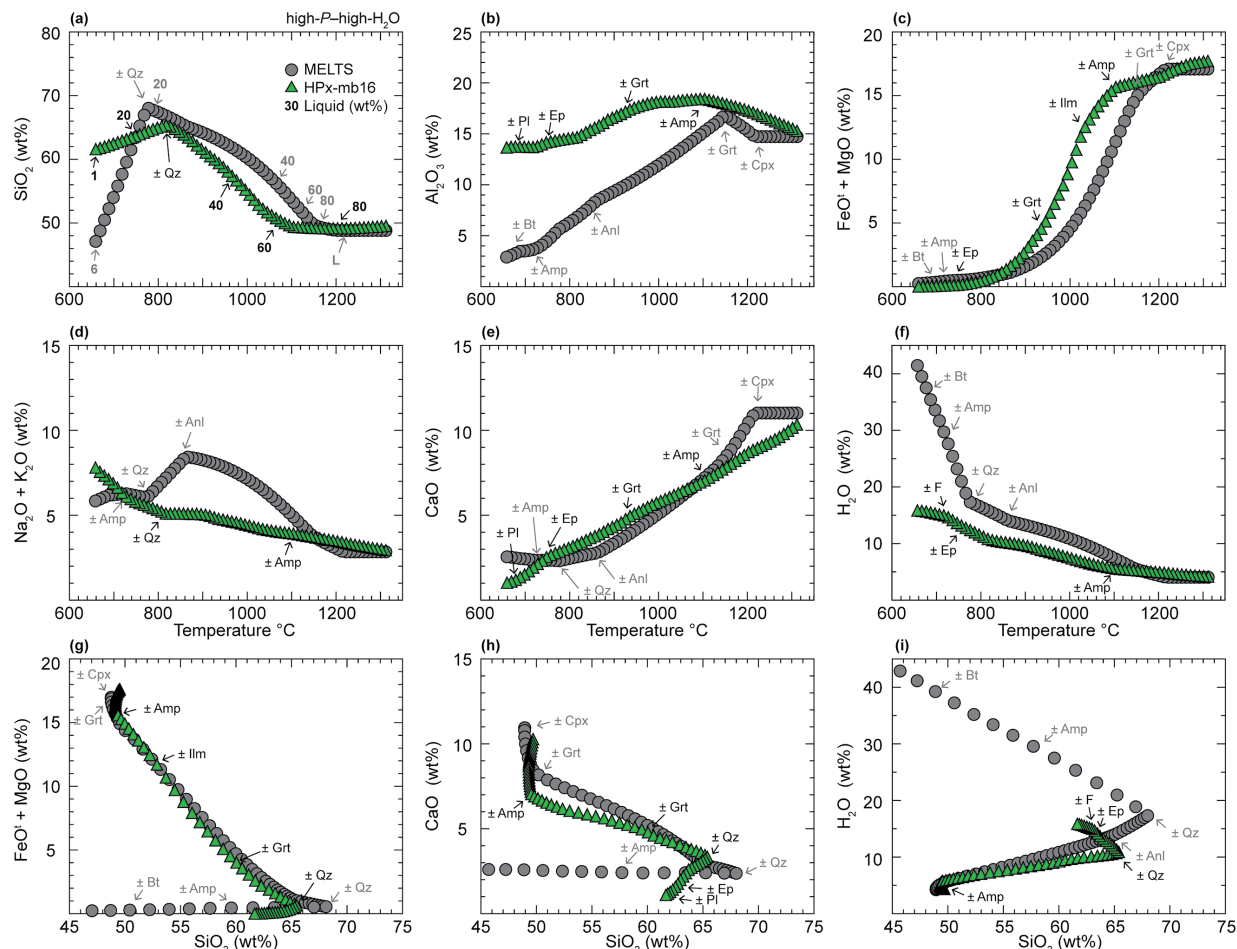


FIGURE 7. Liquid compositional evolution (wt%) at 1 GPa for a high- H_2O (4 wt% H_2O) N-MORB composition. (a–f) Modeled liquid compositions as a function of temperature. (g–i) Modeled liquid compositions shown in Harker diagrams. Approximate liquid fractions (in wt%) are shown in a for comparison between modeling approaches. Mineral abbreviations follow Whitney and Evans (2010) with the exception of “L” and “F” which refer to liquid and fluid, respectively. (Color online.)

complexity and difficulty modeling a – X relations in multisite-multicomponent amphibole phases using available experimental data (Online Materials¹ Table S4). The Si, Mg#, and Ca contents are systematically higher in rhyolite-MELTS than in HPx-mb16 at any given temperature in the high- P –high- H_2O run.

Trace-element signatures of model liquids

Here, we explore the effect of calculated phase relations on the trace-element signatures of the liquids. We used calculated liquid and solid fractions (Online Materials¹ Table S5) along with liquid–mineral partition coefficients to model the liquid trace-element signatures at (1) 900 °C in the low- P –low- H_2O run; (2) 1000 °C in the high- P –low- H_2O run; and (3) 850 °C in the high- P –high- H_2O run. These three scenarios were selected because of the markedly different predicted equilibria between the models. Trace-element modeling was performed at the given state point using mass balance equations found elsewhere (e.g., Shaw 2006; Spera et al. 2007). A wide selection of variably incompatible trace elements was chosen, and partition coefficients were from Bédard (2006) (Online Materials¹ Table S6). To highlight the

similarities and differences in trace element signatures resulting solely from phase assemblage differences, constant liquid–mineral partition coefficients (for each mineral) were used. The starting bulk trace-element composition was that of mean N-MORB from Gale et al. (2013). The results are given in Table 3 and illustrated in normalized incompatible trace-element diagrams and REE diagrams in Figure 8.

In the low- P –low- H_2O run at 900 °C, the stable phase assemblage predicted by rhyolite-MELTS is liquid-plagioclase-orthopyroxene-clinopyroxene-magnetite (Fig. 1c). The calculated liquid trace-element pattern (Figs. 8a and 8b) is relatively enriched in Ta and Zr and depleted in Ba, Pb, Sr, Eu, and Ti. The liquid composition is further characterized by a low-Sr/Y ratio (Sr/Y = 0.44; Table 3), and is not strongly fractionated in REE (La/Yb = 1.86; Table 3). The chondrite-normalized REE pattern shows a strong negative Eu anomaly $\{Eu/Eu^* = [Eu/(Sm \times Nd)^{0.5}] = 0.07$; Table 3}, and is characterized by a flat heavy-REE (HREE) slope (Yb/Gd = 0.62; Table 3). The calculated paragenesis using HPx-mb16 is liquid-plagioclase-amphibole-orthopyroxene-clinopyroxene-ilmenite (Fig. 1c). While the HPx-mb16 liquid compositions

show relatively lower concentrations of all the considered trace elements, most trace elements are similar to those calculated with rhyolite-MELTS. Exceptions are Ta, Gd, and Tb, which are much lower in concentration in HPx-mb16. The liquid composition is characterized by low-Sr/Y ($Sr/Y = 0.76$) and -La/Yb ($La/Yb = 2.26$) ratios (Table 3), a strong Eu negative anomaly ($Eu/Eu^* = 0.12$; Table 3), and a flat HREE slope ($Yb/Gd = 0.78$; Table 3).

In the high-*P*-low-*H*₂O run, the stable phase assemblage at 1000 °C for the rhyolite-MELTS run is liquid-plagioclase-clinopyroxene-garnet (Fig. 2c). The calculated trace-element compositions are shown in Figures 8c and d. The liquid incompatible trace-element pattern is slightly enriched in Ta and Ti but depleted in Ba and Sr and further characterized by a moderate Sr/Y ratio ($Sr/Y = 10.93$; Table 3). It is also strongly fractionated in light to heavy REE ($La/Yb = 35.24$; Table 3) because garnet is a stable phase. The REE pattern does not show a negative Eu anomaly ($Eu/Eu^* = 0.30$; Table 3) and is characterized by a steep HREE slope ($Yb/Gd = 0.18$; Table 3). The paragenesis in HPx-mb16 is liquid-plagioclase-amphibole-orthopyroxene-clinopyroxene-ilmenite (Fig. 2c). The incompatible trace-element pattern of HPx-mb16 is similar to that of rhyolite-MELTS for highly incompatible elements, but there are significant differences in terms of Eu, Gd, Ta, and HREE; the liquid composition is also characterized by a low-Sr/Y ratio ($Sr/Y = 0.80$; Table 3). The REE pattern is not fractionated ($La/Yb = 2.12$; Table 6), shows a strong negative Eu anomaly ($Eu/Eu^* = 0.12$; Table 3), and is enriched in HREE ($Yb/Gd = 0.72$; Table 3).

In the high-*P*-high-*H*₂O run at 850 °C, the paragenesis predicted by MELTS is liquid-clinopyroxene-garnet (Fig. 2d). The calculated trace-element compositions are shown in Figures 8e and 8f. The calculated incompatible trace-element pattern is slightly enriched in Pb, Sr, and Ti and slightly depleted in Th. The liquid composition has a high-Sr/Y ratio ($Sr/Y = 142.48$; Table 3) and is strongly fractionated in LREE/HREE ($La/Yb = 74.96$; Table 3) due to residual garnet. The REE pattern further shows a small positive Eu anomaly ($Eu/Eu^* = 0.48$; Table 3), and is characterized by a steep HREE slope ($Yb/Gd = 0.17$; Table 3). The calculated paragenesis in HPx-mb16 is liquid-amphibole-orthopyroxene-clinopyroxene-garnet-titanite (Fig. 2d). The incompatible trace-element pattern is depleted in highly incompatible elements but enriched in more compatible elements relative to that of the rhyolite-MELTS liquid. The pattern is further characterized by a slight enrichment in Pb, Sr, and Zr and depletion in Ti; the liquid composition has a moderate Sr/Y ratio ($Sr/Y = 12.07$; Table 3). The REE pattern is not fractionated ($La/Yb = 3.54$; Table 3), does not show an Eu negative anomaly ($Eu/Eu^* = 0.37$; Table 3), and is enriched in HREE ($Yb/Gd = 0.81$; Table 3).

Contrasting liquid trace-element signatures: The effect of contrasting mineral assemblages

As discussed in the previous sections, both models yield significant differences in calculated phases and their relative abundances. Unsurprisingly, this directly affects the trace-element signatures of the liquids. For example, partitioning of Ba, Sr, and Eu into plagioclase (Gromet and Silver 1983), means that the increase of plagioclase stability at higher temperatures in HPx-mb16 relative to rhyolite-MELTS and the differences in plagioclase proportion will lead to differences in the concentrations of the Ba, Sr, and Eu

TABLE 3. Liquid trace-element compositions (ppm)

	Low- <i>P</i> -low- <i>H</i> ₂ O at 900 °C		High- <i>P</i> -low- <i>H</i> ₂ O at 1000 °C		High- <i>P</i> -high- <i>H</i> ₂ O at 850 °C	
	MELTS	HPx-mb16	MELTS	HPx-mb16	MELTS	HPx-mb16
Cs	0.21	0.16	0.17	0.14	0.18	0.07
Rb	17.06	13.79	12.72	11.09	13.66	5.57
Ba	39.70	39.44	64.24	40.48	146.95	58.18
Th	1.54	1.40	1.33	1.19	1.52	0.75
U	0.63	0.54	0.51	0.45	0.55	0.25
Nb	21.09	12.29	19.93	11.79	24.43	8.40
Ta	1.96	0.95	1.43	0.90	1.42	0.43
La	18.70	15.62	20.15	15.02	27.93	8.78
Ce	54.97	42.68	54.12	42.09	69.65	20.60
Pb	1.28	1.22	1.84	1.24	3.41	1.37
Pr	8.45	6.04	7.46	6.13	8.96	2.63
Sr	45.66	47.28	99.68	53.04	865.17	265.28
Nd	47.69	29.91	38.52	31.57	43.16	11.22
Zr	684	393	321	365	279	203
Hf	10.23	7.24	7.55	7.13	7.01	3.76
Sm	14.05	7.82	5.75	8.57	4.76	2.70
Eu	1.07	0.99	1.27	1.11	1.58	1.06
Gd	16.17	8.90	3.14	9.81	2.24	3.06
Ti	17755	9095	9800	10354	7479	3522
Tb	2.74	1.55	0.38	1.69	0.26	0.54
Dy	17.52	10.24	1.81	11.09	1.22	3.57
Y	103.38	62.00	9.12	66.60	6.07	21.97
Ho	3.64	2.22	0.30	2.37	0.20	0.79
Er	10.41	6.61	0.72	6.96	0.48	2.33
Tm	1.58	1.05	0.10	1.09	0.06	0.37
Yb	10.07	6.90	0.57	7.07	0.37	2.48
Lu	1.50	1.06	0.08	1.07	0.05	0.39
Ga	32.56	33.25	29.20	34.34	28.97	25.21
Cr	106.69	146.04	48.27	174.84	31.50	110.78
Co	11.29	12.44	34.20	14.97	32.42	11.98
Ni	17.91	25.41	31.55	27.01	42.54	29.74
Cu	92.94	94.91	78.31	92.70	91.97	149.15
Zn	30.87	38.52	34.55	40.03	33.48	61.69
V	461	270	206	299	164	139
Sc	7.77	7.92	5.07	7.61	5.75	7.03
Sr/Y	0.44	0.76	10.93	0.80	142.48	12.07
La/Yb	1.86	2.26	35.24	2.12	74.96	3.54
Yb/Gd	0.62	0.78	0.18	0.72	0.17	0.81
Eu/Eu*	0.07	0.12	0.30	0.12	0.48	0.37

in liquids in equilibrium with their associated crystals at each state point (Fig. 8; Table 3). The considerable effect of the discordant phase equilibria on the trace-element budget is also well illustrated by the contrasting garnet stabilities in the different models. Garnet is more stable in all rhyolite-MELTS calculations, and since it is an important HREE repository (e.g., Bea et al. 1994), its fractionation causes notable HREE depletions in the corresponding rhyolite-MELTS liquid compositions (Fig. 8; Table 3).

The HPx-mb16 trace-element patterns always show negative Ti anomalies, whereas trace-element patterns of rhyolite-MELTS calculations only show negative Ti anomalies in the high-*P*-low-*H*₂O case (Fig. 8; Table 3). The negative Ti anomalies in HPx-mb16 trace-element patterns are controlled by partitioning of Ti into titanite, ilmenite, and amphibole (where present), whereas such phases are never stable in rhyolite-MELTS calculations. In the only example where there is a negative Ti anomaly (Fig. 8; Table 3) in rhyolite-MELTS, the main Ti repository is magnetite.

A key difference in the mineral assemblage predicted by rhyolite-MELTS and HPx-mb16 models is the presence of amphibole. This mineral has relatively high-partition coefficients for MREE and HREE (Online Materials¹ Table S6; Bédard 2006), likely accounting for the depletion in MREE and HREE contents in amphibole-rich HPx-mb16 calculations compared to those of rhyolite-MELTS, as well as to HPx-mb16 calculations with less amphibole (Fig. 8; Table 3).

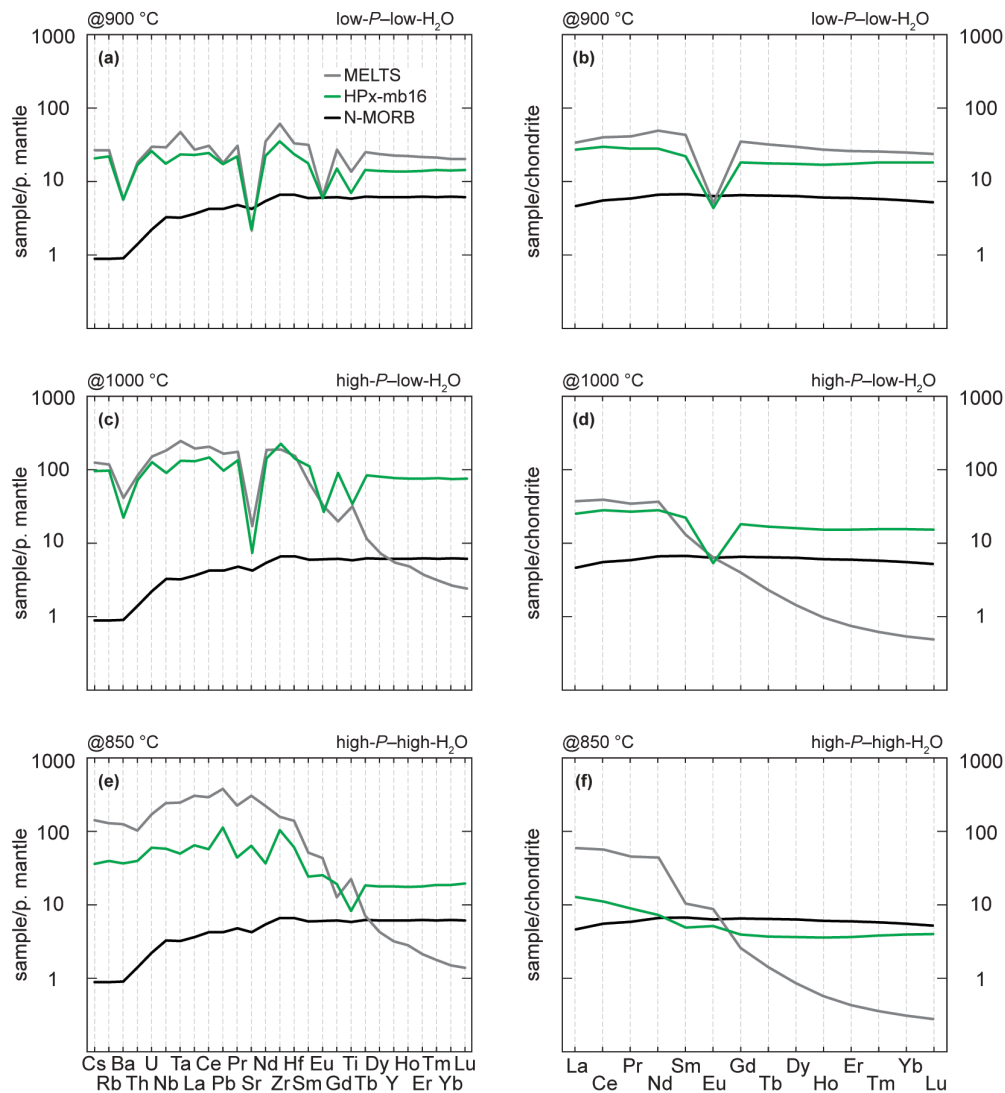


FIGURE 8. Liquid incompatible trace-element patterns at (a–b) 900 °C in the low- P –low- H_2O run, (c–d) 1000 °C in the high- P –low- H_2O run, and (e–f) 850 °C in the high- P –high- H_2O run. (a, c, and e) Shows the normalized to primitive mantle (Sun and McDonough 1989), and (b, d, and f) this shows the normalized to chondrite (McDonough and Sun 1995). The orange line is mean N-MORB from Gale et al. (2013). (Color online.)

Other trace elements (e.g., Cs, Rb, Th, U, and light-REE) are mainly incompatible in the solid phases present in the calculations, thus, the concentrations in the melt are only slightly affected by choice of the thermodynamic model (Fig. 8; Table 3). Rather subtle relative differences in their concentrations can be observed in the high- P –high- H_2O run (Fig. 8; Table 3). Highly incompatible elements may thus generally represent better proxies to model crystallization or anatexis processes with both rhyolite-MELTS and HPx-mb16 since they are less prone to differ significantly with model choice.

COMPARING MODELS TO PETROLOGICAL EXPERIMENTS

To further assess the robustness of the phase equilibria models, we compared model predictions with results from low- and high- P petrological experiments. We selected the experimental

studies of Berndt et al. (2004) and Sen and Dunn (1994) as benchmarks for the comparison. We used the synthetic MORB B1 composition from Berndt et al. (2004) and compared the phase equilibria at 0.2 GPa and 950 and 1000 °C. These conditions correspond to their runs 148 and 153 [Table 3c of Berndt et al. (2004)]. The data in Berndt et al. (2004) were not used in either rhyolite-MELTS or HPx-mb16 calibrations. In addition, we utilized the natural basaltic amphibolite from the Sen and Dunn (1994) experiment and compared the phase equilibria at 1.5 GPa and 975 and 1025 °C. These conditions correspond to their runs B17 and M2 (their Table 2). Although data from Sen and Dunn (1994) were not used to calibrate HPx-mb16, Sen and Dunn data did form a very small part of the data used to calibrate rhyolite-MELTS (Ghiorso et al. 2002). The Berndt et al. (2004) experiments considered oxygen fugacities corresponding to the FMQ buffer, whereas the Sen and Dunn (1994) oxygen fugacity

correspond to $FMQ = +0.5$. Here, for simplicity, calculations with both rhyolite-MELTS and HPx-mb16 were run along the FMQ buffer. Phase proportions from the Berndt et al. (2004) and Sen and Dunn (1994) experiments as well as phase equilibria calculations with rhyolite-MELTS (v1.2.0) and HPx-mb16 are shown in Figure 9 and given in Table 4; experimental and calculated liquid compositions are given in Table 5.

MORB B1 of Berndt et al. (2004)

Phase equilibria at 950 °C slightly differs between the models and experiment 153 (Fig. 9a; Table 4). Liquid, olivine, clinopyroxene, plagioclase, amphibole, and H₂O fluid are observed in the experiment. Rhyolite-MELTS differs from the experiment in that it stabilizes orthopyroxene and a small amount of magnetite but not amphibole. HPx-mb16 stabilizes amphibole, clinopyroxene, and plagioclase as in the experiment but with additional orthopyroxene and a small amount of ilmenite and no olivine. The liquid proportion in the experiment is similar to that predicted in HPx-mb16 but significantly lower in rhyolite-MELTS. Clinopyroxene and plagioclase proportions are relatively similar in HPx-mb16 compared to the experiment; rhyolite-MELTS predicts higher proportions of these phases than both HPx-mb16 and the experiment. The olivine proportion is higher in the rhyolite-MELTS model compared to the experiment. On the other hand, the proportion of amphibole observed in the experiment is similar to that predicted by HPx-mb16. In general, HPx-mb16 is able to better reproduce the phase relations from experiment 153. The rhyolite-MELTS liquid composition is relatively similar to that of the experiment in terms of MgO and CaO contents, whereas the HPx-mb16 liquid composition is in relative agreement with regard to all the other major oxides (Table 5). Significant differences include the MgO and K₂O contents; for instance, the liquid's MgO content in rhyolite-MELTS is within ~5% of the experiment whereas the K₂O content is within ~382% of the experiment. By contrast, the HPx-mb16 calculated MgO content is within ~115% of the experiment, whereas the K₂O content is within ~74% of the experiment. Note that the large relative difference in the K₂O content is exacerbated by low-K₂O contents.

At 1000 °C, the rhyolite-MELTS and HPx-mb16 models,

and the experiment 148 of Berndt et al. (2004) show the same phase assemblage, melt, olivine, clinopyroxene, plagioclase, and H₂O fluid, with the exception of a very small amount of ilmenite that is predicted in HPx-mb16. However, the phase proportions are somewhat different (Fig. 9b; Table 4); both rhyolite-MELTS and HPx-mb16 predict considerably less liquid than observed in the experiment, and both models predict more plagioclase. Rhyolite-MELTS predicts slightly more olivine than measured in the experiment, whereas the HPx-mb16 predicts slightly less olivine than in the experiment. Modeled and experimental clinopyroxene proportions are similar. Overall, rhyolite-MELTS is able to better reproduce the phase equilibria from experiment 148. The HPx-mb16 calculated liquid composition is relatively similar to that of the experiment in terms of SiO₂, Al₂O₃, and H₂O contents, whereas the rhyolite-MELTS liquid composition is in reasonable agreement with the experiment for all the other major oxides (Table 5). Important differences in the compositions include the MgO and K₂O contents; for example, the MgO liquid content in rhyolite-MELTS is within ~3% of the experiment, whereas the liquid's K₂O content is within ~38% of the experiment. On the other hand, the HPx-mb16 calculated liquid MgO content is within ~74% of the experiment and the K₂O content within ~51% of the experiment.

Natural basaltic amphibolite of Sen and Dunn (1994)

The stable phase assemblage in the 975 °C experiment M2 is liquid, clinopyroxene, plagioclase, amphibole, garnet, and rutile. Rhyolite-MELTS model does not stabilize plagioclase, amphibole, or rutile, whereas HPx-mb16 stabilizes the experimental phase assemblage with the exception of plagioclase (Fig. 9c; Table 4). Phase proportions are relatively different between both models and the experiment; the calculated liquid fractions are considerably higher than in the experiment. The calculated clinopyroxene proportion in HPx-mb16 is similar to that in the experiment but considerably higher in rhyolite-MELTS. Similarly, the garnet proportions predicted by both models are significantly higher than in the experiment. The calculated amphibole proportion in HPx-mb16 is relatively less than in the experiment. Rutile occurs as a minor phase in both HPx-mb16

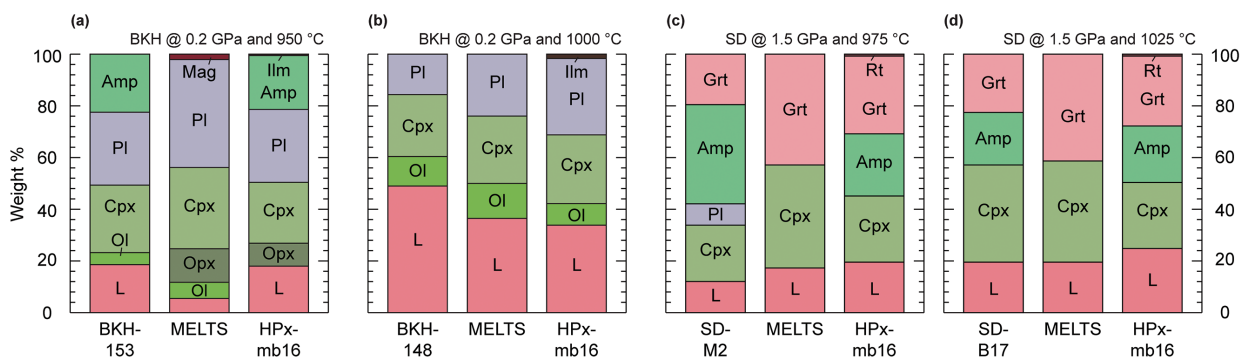


FIGURE 9. Phase proportion comparison experiments of basaltic compositions and model predictions. (a and b) Comparison with Berndt et al. (2004) experiments (BKH). (c and d) Comparison with Sen and Dunn (1994) (SD). Phase proportions are shown on an anhydrous basis (recalculated to 100%). In the SD experiments, rutile is also present as a trace phase. Rhyolite-MELTS models were calculated with rhyolite-MELTS v1.2.0. Mineral abbreviations follow Whitney and Evans (2010) with the exception of “L” and “F” which refer to liquid and fluid, respectively. (Color online.)

TABLE 4. Comparison of phase proportions between experiments of basaltic compositions and model predictions (wt%)

	0.2 GPa and 950 °C					0.2 GPa and 1000 °C					1.5 GPa and 975 °C					1.5 GPa and 1025 °C				
	BKH (153)	MELTS	HPx- mb16	% diff. ^a	% diff. ^b	BKH (148)	MELTS	HPx- mb16	% diff. ¹	% diff. ²	SD (M2)	MELTS	HPx- mb16	% diff. ^a	% diff. ^b	SD (B17)	MELTS	HPx- mb16	% diff. ^a	% diff. ^b
L	19	6	18	-70	-3	49	37	33	-25	-31	12	17	20	40	61	20	19	25	-2	27
Ol	5	6	-	29	-	11	14	9	19	-24	-	-	-	-	-	-	-	-	-	-
Opx	-	13	9	-	-	-	-	-	-	-	-	-	-	-	-	-	-	-	-	-
Cpx	26	31	24	21	-9	24	26	27	8	10	21	40	26	89	21	37	40	25	6	-32
Pl	29	42	28	47	-1	16	24	30	53	90	9	-	-	-	-	-	-	-	-	-
Amp	22	-	21	-	-8	-	-	-	-	-	39	-	24	-	-39	20	-	22	-	8
Ilm	-	-	<1	-	-	-	-	2	-	-	-	-	-	-	-	-	-	-	-	-
Mag	-	2	-	-	-	-	-	-	-	-	-	-	-	-	-	-	-	-	-	-
Grt	-	-	-	-	-	-	-	-	-	-	19	43	30	122	58	23	41	27	81	19
Rt	-	-	-	-	-	-	-	-	-	-	tr	-	<1	-	-	tr	-	<1	-	-

Notes: tr = trace; BKH = Berndt et al. (2004); SD = Sen and Dunn (1994). Mineral abbreviations follow Whitney and Evans (2010) with the exception of "L" which refers to liquid. Phase proportions are shown in an anhydrous basis (recalculated to 100%).

^a Difference between the experiment and MELTS.

^b Difference between the experiment and HPx-mb16.

and the experiment. In general, HPx-mb16 better reproduces the phase relations at 975 °C. The rhyolite-MELTS liquid composition is relatively similar to that of the experiment in terms of FeO^l and MgO liquid contents, whereas the HPx-mb16 liquid composition is in relative agreement with the experiment for all the other major oxides (Table 5). Significant differences include the FeO^l and K₂O contents; for instance, the FeO^l liquid content in rhyolite-MELTS is within ~29% of the experiment, whereas the liquid K₂O content is within ~86% of the experiment. On the other hand, the HPx-mb16 calculated FeO^l liquid content is within ~73% of the experiment, and the K₂O content is within ~32% of the experiment.

The observed phase assemblage at 1025 °C in the Sen and Dunn (1994) experiment B17 is liquid, clinopyroxene, amphibole, garnet, and rutile. HPx-mb16 predicts the same phases, whereas rhyolite-MELTS differs from the experiment in that it stabilizes neither amphibole nor rutile. Proportions of most other phases are fairly similar between the computed models and the experiment, although HPx-mb16 predicts relatively more liquid and less clinopyroxene (Fig. 9d; Table 4). The proportion of garnet calculated with rhyolite-MELTS is considerably higher than in the experiment, whereas HPx-mb16 predicts less garnet than rhyolite-MELTS but more than the experiment. The amphibole proportion observed in the experiment is similar to that predicted by HPx-mb16. Rutile occurs as a minor phase in both HPx-mb16 and the experiment. In general, HPx-mb16 better reproduces the phase relations of experiment B17. The rhyolite-MELTS liquid composition is relatively similar to that of the experiment in terms of SiO₂, FeO^l, and MgO contents, whereas the HPx-mb16 liquid composition is in relative agreement with all other major element oxides (Table 5). Important differences include the FeO^l and Na₂O contents; for example, the FeO^l liquid content in rhyolite-MELTS is within ~32% of the experiment, whereas the liquid Na₂O content is within ~79% of the experiment. By contrast, the HPx-mb16 calculated FeO^l is within ~78% of the experiment, and the liquid's Na₂O content is within ~1% of the experiment.

DISCUSSION

Although a minor oxide and therefore not as important as many of the major element oxides, the lack of the TiO₂ component in the Green et al. (2016) liquid *a-X* relations precludes accurately

modeling phase equilibria at or near liquidus conditions using HPx-mb16 in the NCKFMASHTO system. As TiO₂ cannot be incorporated into the liquid, there is always a Ti-bearing stable phase at high-*T*; this, in turn, affects the overall phase equilibria, including the liquid compositions. For instance, rhyolite-MELTS predicts the liquidus at ~1340–1100 °C, whereas the HPx-mb16 model is unable to model these conditions; clinopyroxene and/or plagioclase and a Ti-bearing phase are already present at the liquidus conditions predicted by rhyolite-MELTS (Figs. 1 and 2). Recently, Holland et al. (2018) and Tomlinson and Holland (2021) published *a-X* relations for relevant crystalline solutions enabling modeling of peridotitic to granitic liquids. This set of *a-X* relations includes more complex liquid and clinopyroxene *a-X* relations (including TiO₂ and Fe₂O₃ in the liquid and TiO₂ and K₂O in the clinopyroxene) than in the *a-X* relations from HPx-mb16. In the first instance, this set of *a-X* relations might represent a better approach to modeling suprasolidus processes than HPx-mb16; yet, a recent study indicates that phase equilibria calculated with the Holland et al. (2018) relations are not significantly different from calculations performed with HPx-mb16; moreover, HPx-mb16 produces similar compositions and better reproduces the FeO^l and MgO liquid contents from experiments than the Holland et al. (2018) *a-X* relations (García-Arias 2020).

When comparing our model predictions to experiments, rhyolite-MELTS and HPx-mb16 better reproduce phase equilibria within the *P-T* conditions in which they were calibrated to be used. The phase equilibria predicted by rhyolite-MELTS are broadly similar to the high-*T* experiments compared to those predicted by HPx-mb16 (Fig. 9; Tables 4 and 5); by contrast, at temperatures less than ~1000 °C, HPx-mb16 provides more robust liquid-present phase equilibria (Fig. 9; Tables 4 and 5) as it better reproduces the considered experiments compared to rhyolite-MELTS. Importantly, as shown in some works (e.g., White et al. 2007; Green et al. 2016), HPx-mb16 is able to accurately capture subsolidus equilibria.

One of the key differences between the rhyolite-MELTS and HPx-mb16 models is how H₂O is partitioned in the liquid and hydroxyl (OH⁻) in the crystalline phases. Amphibole is predicted in HPx-mb16 calculations, whereas amphibole stability and modal abundance are quite limited in rhyolite-MELTS (Figs. 1 and 2; Table 2). In the calculations presented here, rhyolite-MELTS partitions H₂O into liquid and/or analcime and/or a coexisting fluid

TABLE 5. Comparison of liquid compositions between experiments of basaltic compositions and model predictions (wt%)

	0.2 GPa and 950 °C					0.2 GPa and 1000 °C					1.5 GPa and 925 °C					1.5 GPa and 1025 °C				
	BKH (153)	MELTS	HPx- mb16	% diff. ^a	% diff. ^b	BKH (148)	MELTS	HPx- mb16	% diff. ^a	% diff. ^b	SD (M2)	MELTS	HPx- mb16	% diff. ^a	% diff. ^b	SD (B17)	MELTS	HPx- mb16	% diff. ^a	% diff. ^b
L fraction (wt%)	19	6	18	-70	-3	49	37	33	-25	-31	12	17	20	40	61	20	19	25	-2	27
SiO ₂	55.77	59.67	55.60	7	0	50.83	54.83	53.90	8	6	65.29	67.33	63.18	3	-3	62.82	65.50	59.66	4	-5
TiO ₂	1.13	0.30	-	-74	-	1.19	0.52	-	-56	-	0.76	0.39	-	-49	-	1.06	0.51	-	-52	-
Al ₂ O ₃	16.78	14.10	14.48	-16	-14	18.37	15.73	15.00	-14	-18	18.53	12.25	18.16	-34	-2	18.36	12.89	17.55	-30	-4
FeO ^l	8.56	4.89	10.96	-43	28	8.16	7.46	10.85	-9	33	2.85	2.02	4.93	-29	73	4.81	3.27	8.58	-32	78
MgO	2.40	2.28	5.16	-5	115	3.61	3.70	6.29	3	74	0.72	0.54	1.21	-25	68	1.29	0.75	2.15	-42	66
CaO	6.30	4.72	3.19	-25	-49	9.10	7.36	4.28	-19	-53	2.63	2.13	3.11	-19	18	3.52	2.72	3.73	-23	6
Na ₂ O	3.96	6.62	5.80	67	46	3.75	4.48	5.22	19	39	6.49	10.26	5.81	58	-10	5.53	9.88	5.48	79	-1
K ₂ O	0.22	1.06	0.38	382	74	0.15	0.21	0.23	38	51	2.73	5.08	3.59	86	32	2.61	4.48	2.86	72	9
H ₂ O	4.88	6.36	4.42	30	-10	4.83	5.71	4.22	18	-13	-	-	-	-	-	-	-	-	-	-
Total	100	100	100			100	100	100			100	100	100			100	100	100		

Notes: tr = trace; BKH = Berndt et al. (2004); SD = Sen and Dunn (1994); L = liquid.

^a Difference between the experiment and MELTS.

^b Difference between the experiment and HPx-mb16.

phase (Figs. 1 and 2; Table 2). These results illustrate the acknowledged limitation of rhyolite-MELTS in modeling amphibole (and biotite)-bearing phase equilibria (<http://melts.ofm-research.org/>; Ghiorso and Gualda 2015). The HPx-mb16 model may therefore be the best choice to model equilibrium melting and crystallization in scenarios where significant amounts of modal amphibole are observed or predicted.

While not considered in our present study, the use of the HPx-mb16 model to study fractional crystallization or any other open-system process would be relatively laborious for this task with the current software available (i.e., Theriak-Domino, *Perple_X*, and THERMOCALC), although several works using this software have successfully modeled open-system processes (e.g., Yakymchuk and Brown 2014; Kendrick and Yakymchuk 2020; Stuck and Diener 2018; Johnson et al. 2021; Hernández-Montenegro et al. 2021)

Furthermore, it is important to note that a recent comparative study assessing the robustness of the Green et al. (2016) clinopyroxene and amphibole *a-X* relations shows discrepancies between the phase equilibria calculations and natural rocks in the proportions and compositions (Forshaw et al. 2019; Santos et al. 2019); yet, our comparisons with the experiments show that the difference in proportions is not as significant as suggested in those studies. We argue that these different outcomes may be related to different bulk-rock compositions used in the comparisons.

IMPLICATIONS

From the examples presented here, the lesson is clear: the modeling tool choice and an understanding of model constraints, uncertainties, and the similarities (and differences) among models are critical to accurately convey the geological implications of a computational result. Below, we highlight selected examples of how model choice can influence geologic interpretations. The examples cited below are illustrative since we only present a small subset of possible compositions and conditions, and yet, the underlying principal conclusion likely remains relevant to all model-based studies of the magmatic evolution of the crust and upper mantle.

HPx-mb16 and rhyolite-MELTS yield distinctly different mineral assemblages for some of the runs. For example, at 850 °C in the low-*P*-high-*H*₂O run, the crystalline phases in equilibrium with liquid predicted by rhyolite-MELTS correspond

to a granulitic assemblage, whereas in HPx-mb16, an amphibolite-like assemblage is predicted (Figs. 1b and 1d). Similarly, at 800 °C in the high-*P*-low-*H*₂O run, rhyolite-MELTS predicts a plagioclase-bearing garnet pyroxenite crystalline assemblage, whereas HPx-mb16 predicts a garnet amphibolite crystalline assemblage (Figs. 2a and 2c; Table 2). As a consequence of the difference in amphibole stability, the distribution of H₂O content among solid phases is different depending on the modeling tool. This has important implications for modeling crustal anatexis and growth processes. For example, the fertility (i.e., the potential to melt) of these solid assemblages will differ significantly; amphibole dehydration melting of the amphibolitic cumulate would promote greater liquid fractions (for the same pressure and temperature conditions) compared to the dry granulitic and/or pyroxenite cumulate; different modeling approaches will lead to different volumes of liquid, and thus in different crustal growth rates. The differences in the calculated phases can also affect petrophysical properties such as density, seismic velocities, and thermal conductivity (e.g., Carlson and Miller 2004; Whittington et al. 2009). For example, at 900 °C in the high-*P*-high-*H*₂O run (Figs. 2a and 2c; Table 2), the dry crystalline assemblage predicted by rhyolite-MELTS (i.e., the garnet pyroxenite) has a significantly higher density ($\rho = 3.59 \text{ g/cm}^3$) than the hydrated mineral assemblage predicted by the HPx-mb16 model ($\rho = 2.82 \text{ g/cm}^3$); such differences may influence interpretations invoking crustal foundering via gravitational instabilities which in turn may drastically affect the compositional stratification of the crust. Differences in thermal diffusivity would also be expected between the hydrous and anhydrous mineral assemblages, which would affect heat flow and the associated local geotherms. Thus, the choice of modeling approach may yield different interpretations for the development of chemical stratification of continental crust, the potential for crustal delamination, and the thermal and rheological crustal structure.

Observed differences between the calculated liquid compositions may have important implications for forward modeling of igneous processes. For instance, different calculated melt compositions may lead to distinct liquid lines of descent representing different magma series (Fig. 3; e.g., Carmichael et al. 1974). In the low-*P*-high-*H*₂O run, the HPx-mb16 liquid composition produced by equilibrium crystallization follows a subalkaline tholeiitic trend, whereas the liquid calculated with

rhyolite-MELTS evolves first along a subalkaline trend but then follows an alkaline series trend when equilibrium crystallization is >50% complete (Fig. 3b). These model differences could lead to differences in, for example, hypotheses about tectonic setting. Furthermore, our results show that calculated liquid compositions diverge more at near-solidus temperatures, the difference being greater in the high-*P* calculations (Fig. 3). These differences have implications for modeling processes such as crustal assimilation because the composition of small degree (near solidus) anatectic melts can have a profound impact on the major and trace element, isotopic, and phase equilibria signatures of crustally contaminated magmas (e.g., Bohrsen et al. 2014). Our results therefore concur with the recognized limitation of thermodynamic modeling at “lower” temperatures, particularly using rhyolite-MELTS (<http://melts.ofm-research.org/>) (e.g., rhyolite-MELTS is suggested to perform best when a silicate liquid is present in the phase assemblage, as illustrated in comparison with the experiments (Fig. 9; Tables 4 and 5).

The difference in the calculated liquid compositions coupled with the calculated solid fractions may significantly impact the interpretation of tonalite-trondhjemite-granodiorite (TTGs) and adakite petrogenesis. The major elements commonly used to identify and classify TTGs and adakites (e.g., high Mg# and low K₂O/Na₂O) are some of the elements that vary the most between the models. (Figs. 4–7), complicating their use in documenting the petrogenesis of such rocks (e.g., Moyen 2011; Palin et al. 2016; Hernández-Uribe et al. 2020). The solid assemblage controls the trace-element liquid signature, which has been considered diagnostic of the source depth and composition of the liquid (Moyen and Martin 2012). TTGs are subdivided into high-, medium-, and low-pressure groups based on the Sr/Y and La/Yb ratios, which are controlled by garnet, plagioclase, rutile, and amphibole stabilities (Moyen 2011; Moyen and Martin 2012). According to our results, the presence or absence, and abundance of such phases may vary substantially between the two thermodynamic models examined here (Figs. 1 and 2; Table 2). For example, garnet stability is increased in rhyolite-MELTS compared to HPx-mb16, whereas plagioclase stability is expanded to higher temperatures in HPx-mb16 but generally predicted in lower proportions (Figs. 1 and 2). Such differences could easily lead to contrasting trace-element signatures (Table 3) and thus result in different explanations for tectonic environments of formation for TTGs (e.g., slab melting during subduction vs. melting of a thickened crust; Martin et al. 2014; Palin et al. 2016; Johnson et al. 2017). This emphasizes the need for careful consideration of model limitations and uncertainties.

Statements about model performance are nuanced and must be thoughtfully considered depending on the particular application under study, including the inherent geological uncertainties not associated with the thermodynamic model per se. There may be cases where the geological uncertainties are larger than the model uncertainties or vice versa. A careful parsing of all uncertainties—intermodel, intramodel, and geologic—is critical when applying thermodynamic models to Earth systems.

The comparisons presented in this study are illustrative, not exhaustive. We performed equilibrium modeling using a single bulk composition (N-MORB) over a modest range of pressures and bulk H₂O contents. We did not consider fractional or open-

system processes or other redox conditions; such comparisons are outside of the scope of a single paper. In felsic and/or open systems, which often show considerably higher degrees of geochemical heterogeneity, the differences between the models may be larger, especially when amphibole and sheet silicate crystalline solutions are more abundant. We hope our work spurs additional work, including further comparative examination of other thermodynamic conditions (composition, volatiles, redox, pressure, phase assemblages) and models.

From our limited set of comparative calculations, there are three major points. The first is that our results show how the choice of petrological modeling tool can influence conclusions about associated geological processes. We have shown that for the same model input (e.g., *P-T-H₂O*), the model choice may lead to different interpretations of crustal structure, density, and melting systematics. The second point is that different models are better suited to modeling different *P-T* ranges and that studies such as ours are needed to highlight these differences for users more comprehensively. For example, HPx-mb16 is likely better suited for modeling water-rich systems with hydrous mineral phases (e.g., volcanic arc settings) at lower temperatures, whereas rhyolite-MELTS may work better for drier systems at lower pressures and higher temperatures (e.g., MORB and OIB's). Third, our work illustrates the importance of using multiple petrological indicators to assess the efficacy of one model vs. another. Major- and trace-element and isotopic compositions of mineral phases, as well as mineral proportions, can enhance the choice of a best-fit model compared to using melt compositional data only.

While the current thermodynamic databases and *a-X* relations for solid-solution phases used in the igneous and metamorphic petrology communities provide a framework for forward modeling of important igneous and metamorphic processes, the ultimate goal should be to develop an internally consistent thermodynamic database and *a-X* relations applicable to both subsolidus metamorphic processes as well as suprasolidus igneous and metamorphic processes. This methodological development should proceed hand-in-hand with new petrological experiments that fill the current gap in knowledge (especially at high-pressure conditions) and with a development of a user-friendly software with the capability to model the range of closed and open-system processes that are relevant to igneous and metamorphic systems (e.g., equilibrium/fractional melting/crystallization and crustal assimilation). In parallel with model development and enhancement, systematic comparative studies—such as the one presented here—are necessary to thoroughly assess and test predictions from different models and to compare to experimental and natural data. We hope our study provokes others to continue to explore the strengths and weaknesses of the available multicomponent and multiphase phase equilibria tools.

ACKNOWLEDGMENTS AND FUNDING

D. Hernández-Uribe thanks M. Konrad-Schmölke and J.D. Hernández-Montenegro for help with Theriak-Domino calculations. F.J. Spera acknowledges the support of the U.S. National Science Foundation over the past fifty years. W.A. Bohrsen received funding for this project from the U.S. National Science Foundation and the Colorado School of Mines. The contribution of J.S. Heinonen was supported by the Academy of Finland Grant 295129. Reviews by J. Brian Balta and J. Diener greatly improved the manuscript and are gratefully acknowledged. A. Acosta-Vigil is thanked for editorial handling.

REFERENCES CITED

- Asimow, P.D., and Ghiorso, M.S. (1998) Algorithmic modifications extending MELTS to calculate subsolidus phase relations. *American Mineralogist*, 83, 1127–1132.
- Asimow, P.D., Dixon, J.E., and Langmuir, C.H. (2004) A hydrous melting and fractionation model for mid-ocean ridge basalts: Application to the Mid-Atlantic Ridge near the Azores. *Geochemistry, Geophysics, Geosystems*, 5, Q01E16.
- Balta, J.B., and McSween, H.Y. Jr. (2013) Application of the MELTS algorithm to Martian compositions and implications for magma crystallization. *Journal of Geophysical Research: Planets*, 118, 2502–2519.
- Bartoli, O., and Carvalho, B.B. (2021) Anatectic granites in their source region: A comparison between experiments, thermodynamic modelling and nanogranitoids. *Lithos*, 402–403, 106046.
- Bea, F., Pereira, M. D., and Stroh, A. (1994) Mineral/leucosome trace-element partitioning in a peraluminous migmatite (a laser ablation-ICP-MS study). *Chemical Geology*, 117(1–4), 291–312.
- Bédard, J.H. (2006) A catalytic delamination-driven model for coupled genesis of Archaean crust and sub-continental lithospheric mantle. *Geochimica et Cosmochimica Acta*, 70, 1188–1214.
- Berman, R.G. (1988) Internally-consistent thermodynamic data for minerals in the system $\text{Na}_2\text{O}-\text{K}_2\text{O}-\text{CaO}-\text{MgO}-\text{FeO}-\text{Fe}_2\text{O}_3-\text{Al}_2\text{O}_3-\text{SiO}_2-\text{TiO}_2-\text{H}_2\text{O}-\text{CO}_2$. *Journal of Petrology*, 29, 445–522.
- (1990) Mixing properties of Ca-Mg-Fe-Mn garnets. *American Mineralogist*, 75, 328–344.
- Berman, R.G., and Brown, T.H. (1985) Heat capacity of minerals in the system $\text{Na}_2\text{O}-\text{K}_2\text{O}-\text{CaO}-\text{MgO}-\text{FeO}-\text{Fe}_2\text{O}_3-\text{Al}_2\text{O}_3-\text{SiO}_2-\text{TiO}_2-\text{H}_2\text{O}-\text{CO}_2$: representation, estimation, and high temperature extrapolation. *Contributions to Mineralogy and Petrology*, 89, 168–183.
- Berman, R.G., and Koziol, A.M. (1991) Ternary excess properties of grossular-pyrope-almandine garnet and their influence in geothermobarometry. *American Mineralogist*, 76, 1223–1231.
- Berndt, J., Koepke, J., and Holtz, F. (2004) An experimental investigation of the influence of water and oxygen fugacity on differentiation of MORB at 200 MPa. *Journal of Petrology*, 46, 135–167.
- Bohrson, W.A., Spera, F.J., Ghiorso, M.S., Brown, G.A., Creamer, J.B., and Mayfield, A. (2014) Thermodynamic model for energy-constrained open-system evolution of crustal magma bodies undergoing simultaneous recharge, assimilation and crystallization: The magma chamber simulator. *Journal of Petrology*, 55, 1685–1717.
- Bohrson, W.A., Spera, F.J., Heinonen, J.S., Brown, G.A., Scruggs, M.A., Adams, J.V., Takach, M., Zeff, G., and Suikkanen, E. (2020) Diagnosing open-system magmatic processes using the Magma Chamber Simulator (MCS): part I—Major elements and phase equilibria. *Contributions to Mineralogy and Petrology*, 175, 104.
- Bowen, N.L. (1928) *The Evolution of the Igneous Rocks*. Princeton University Press, New Jersey.
- (1945) Phase equilibria bearing on the origin and differentiation of alkaline rocks. *American Journal of Science*, 243, 75–89.
- Brown, M. (2007) Crustal melting and melt extraction, ascent and emplacement in orogens: mechanisms and consequences. *Journal of the Geological Society*, 164, 709–730.
- Carlson, R.L., and Miller, D.J. (2004) Influence of pressure and mineralogy on seismic velocities in oceanic gabbros: Implications for the composition and state of the lower oceanic crust. *Journal of Geophysical Research: Solid Earth*, 109, B09205.
- Carmichael, I.S., Turner, F.J., and Verhoogen, J. (1974) *Igneous Petrology*, 739 p. McGraw-Hill.
- Connolly, J.A. (2005) Computation of phase equilibria by linear programming: a tool for geodynamic modeling and its application to subduction zone decarbonation. *Earth and Planetary Science Letters*, 236, 524–541.
- de Capitani, C., and Brown, T.H. (1987) The computation of chemical equilibrium in complex systems containing non-ideal solutions. *Geochimica et Cosmochimica Acta*, 51, 2639–2652.
- de Capitani, C., and Petrakakis, K. (2010) The computation of equilibrium assemblage diagrams with Theriak/Domino software. *American Mineralogist*, 95, 1006–1016.
- Elkins, L.T., and Grove, T.L. (1990) Ternary feldspar experiments and thermodynamic models. *American Mineralogist*, 75, 544–559.
- England, P.C., and Thompson, A. (1986) *Some thermal and tectonic models for crustal melting in continental collision zones*. Geological Society, London, Special Publications, 19, 83–94.
- Essene, E.J. (1989) The current status of thermobarometry in metamorphic rocks. In J.S. Daly, R.A. Cliff, and B.W.D. Yardley, Eds., *Evolution of Metamorphic Belts*. Geological Society, London, Special Publications, 43, 1–44.
- Forshaw, J.B., Waters, D.J., Pattison, D.R., Palin, R.M., and Gopon, P. (2019) A comparison of observed and thermodynamically predicted phase equilibria and mineral compositions in mafic granulites. *Journal of Metamorphic Geology*, 37, 153–179.
- Fowler, S.J., and Spera, F.J. (2010) A metamodal model for crustal magmatism: Phase equilibria of giant ignimbrites. *Journal of Petrology*, 51, 1783–1830.
- Gale, A., Dalton, C.A., Langmuir, C.H., Su, Y., and Schilling, J.G. (2013) The mean composition of ocean ridge basalts. *Geochemistry, Geophysics, Geosystems*, 14, 489–518.
- García-Arias, M. (2020) Consistency of the activity–composition models of Holland, Green, and Powell (2018) with experiments on natural and synthetic compositions: A comparative study. *Journal of Metamorphic Geology*, 39, 993–1010.
- García-Arias, M., and Stevens, G. (2017) Phase equilibrium modelling of granite magma petrogenesis: A. An evaluation of the magma compositions produced by crystal entrapment in the source. *Lithos*, 277, 131–153.
- Gervais, F., and Trapy, P.H. (2021) Testing solution models for phase equilibrium (forward) modeling of partial melting experiments. *Contributions to Mineralogy and Petrology*, 176, 1–18.
- Ghiorso, M.S. (1990) Thermodynamic properties of hematite-ilmenite-geikielite solid solutions. *Contributions to Mineralogy and Petrology*, 104, 645–667.
- (2004) An equation of state for silicate melts. I. Formulation of a general model. *American Journal of Science*, 304(8–9), 637–678.
- Ghiorso, M.S., and Evans, B.W. (2008) Thermodynamics of rhombohedral oxide solid solutions and a revision of the Fe-Ti two-oxide geothermometer and oxygen-barometer. *American Journal of Science*, 308(9), 957–1039.
- Ghiorso, M.S., and Gualda, G.A. (2015) An $\text{H}_2\text{O}-\text{CO}_2$ mixed fluid saturation model compatible with rhyolite-MELTS. *Contributions to Mineralogy and Petrology*, 169, 1–30.
- Ghiorso, M.S., and Sack, O. (1991) Fe-Ti oxide geothermometry: thermodynamic formulation and the estimation of intensive variables in silicic magmas. *Contributions to Mineralogy and Petrology*, 108, 485–510.
- (1995) Chemical mass transfer in magmatic processes IV. A revised and internally consistent thermodynamic model for the interpolation and extrapolation of liquid-solid equilibria in magmatic systems at elevated temperatures and pressures. *Contributions to Mineralogy and Petrology*, 119, 197–212.
- Ghiorso, M.S., Evans, B.W., Hirschmann, M.M., and Yang, H. (1995) Thermodynamics of the amphiboles: Fe-Mg cummingtonite solid solutions. *American Mineralogist*, 80, 502–519.
- Ghiorso, M.S., Hirschmann, M.M., Reiners, P.W., and Kress, V. (2002) The pMELTS: An revision of MELTS aimed at improving calculation of phase relations and major element partitioning involved in partial melting of the mantle at pressures up to 3 GPa. *Geochemistry, Geophysics, Geosystems*, 3, 1–35.
- Green, E.C.R., White, R.W., Diener, J.F.A., Powell, R., Holland, T.J.B., and Palin, R.M. (2016) Activity–composition relations for the calculation of partial melting equilibria in metabasic rocks. *Journal of Metamorphic Geology*, 34, 845–869.
- Gromet, L.P., and Silver, L.T. (1983) Rare earth element distributions among minerals in a granulite and their petrogenetic implications. *Geochimica et Cosmochimica Acta*, 47(5), 925–939.
- Gualda, G.A., Ghiorso, M.S., Lemons, R.V., and Carley, T.L. (2012) Rhyolite-MELTS: A modified calibration of MELTS optimized for silica-rich, fluid-bearing magmatic systems. *Journal of Petrology*, 53, 875–890.
- Guevara, V.E., and Caddick, M.J. (2016) Shooting at a moving target: Phase equilibria modelling of high-temperature metamorphism. *Journal of Metamorphic Geology*, 34, 209–235.
- Heinonen, J.S., Luttinen, A.V., Spera, F.J., and Bohrson, W.A. (2019) Deep open storage and shallow closed transport system for a continental flood basalalt sequence revealed with Magma Chamber Simulator. *Contributions to Mineralogy and Petrology*, 174, 87.
- Hernández-Montenegro, J.D., Palin, R.M., Zuluaga, C.A., and Hernández-Uribe, D. (2021) Archean continental crust formed by magma hybridization and voluminous partial melting. *Scientific Reports*, 11, 1–9.
- Hernández-Uribe, D., and Palin, R.M. (2019) A revised petrological model for subducted oceanic crust: insights from phase equilibria modeling. *Journal of Metamorphic Geology*, 37, 745–768.
- Hernández-Uribe, D., Hernández-Montenegro, J.D., Cone, K.A., and Palin, R.M. (2020) Oceanic slab-top melting during subduction: Implications for trace-element recycling and adakite petrogenesis. *Geology*, 48, 216–220.
- Hirschmann, M.M., Ghiorso, M.S., Wasylenki, L.E., Asimow, P.D., and Stolper, E.M. (1998) Calculation of peridotite partial melting from thermodynamic models of minerals and melts. I. Review of methods and comparison with experiments. *Journal of Petrology*, 39, 1091–1115.
- Holland, T.J.B., and Powell, R. (1998) An internally consistent thermodynamic data set for phases of petrological interest. *Journal of Metamorphic Geology*, 16, 309–343.
- (2001) Calculation of phase relations involving haplogranitic melts using an internally consistent thermodynamic dataset. *Journal of Petrology*, 42, 673–683.
- (2003) Activity–composition relations for phases in petrological calculations: an asymmetric multicomponent formulation. *Contributions to Mineralogy and Petrology*, 145, 492–501.
- (2011) An improved and extended internally consistent thermodynamic dataset for phases of petrological interest, involving a new equation of state for solids. *Journal of Metamorphic Geology*, 29, 333–383.
- Holland, T.J., Green, E.C., and Powell, R. (2018) Melting of peridotites through to granites: a simple thermodynamic model in the system KNCFMASHTOCr. *Journal of Petrology*, 59, 881–900.
- Jennings, E.S., and Holland, T.J. (2015) A simple thermodynamic model for melting of peridotite in the system NCFMASOCr. *Journal of Petrology*, 56, 869–892.
- Johnson, T.E., White, R.W., and Powell, R. (2008) Partial melting of metagreywacke: a calculated mineral equilibria study. *Journal of Metamorphic Geology*, 26, 837–853.
- Johnson, T.E., Brown, M., Gardiner, N.J., Kirkland, C.L., and Smithies, R.H. (2017)

- Earth's first stable continents did not form by subduction. *Nature*, 543, 239–242.
- Johnson, T.E., Morrissey, L.J., Nemchin, A.A., Gardiner, N.J., and Snape, J.F. (2021) The phases of the Moon: Modelling crystallisation of the lunar magma ocean through equilibrium thermodynamics. *Earth and Planetary Science Letters*, 556, 116721.
- Kendrick, J., and Yakymchuk, C. (2020) Garnet fractionation, progressive melt loss and bulk composition variations in anatectic metabasites: complications for interpreting the geodynamic significance of TTGs. *Geoscience Frontiers*, 11, 745–763.
- Kerrick, D.M., and Connolly, J.A.D. (2001) Metamorphic devolatilization of subducted oceanic metabasalts: implications for seismicity, arc magmatism and volatile recycling. *Earth and Planetary Science Letters*, 189, 19–29.
- Korhonen, F.J., Clark, C., Brown, M., and Taylor, R.J.M. (2014) Taking the temperature of Earth's hottest crust. *Earth and Planetary Science Letters*, 408, 341–354.
- Lanari, P., and Duisterhoef, E. (2019) Modeling metamorphic rocks using equilibrium thermodynamics and internally consistent databases: Past achievements, problems and perspectives. *Journal of Petrology*, 60, 19–56.
- Le Bas, M.J., Maitre, R.W.L., Streckeisen, A., Zanettin, B., and IUGS Subcommittee on the Systematics of Igneous Rocks (1986) A chemical classification of volcanic rocks based on the total alkali-silica diagram. *Journal of Petrology*, 27, 745–750.
- Martin, H., Moyen, J.F., Guitreau, M., Blichert-Toft, J., and Le Pennec, J.L. (2014) Why Archaean TTG cannot be generated by MORB melting in subduction zones. *Lithos*, 198–199, 1–13.
- McDonough, W.F., and Sun, S.S. (1995) The composition of the Earth. *Chemical Geology*, 120, 223–253.
- Moyen, J.F. (2009) High Sr/Y and La/Yb ratios: the meaning of the “adakitic signature.” *Lithos*, 112, 556–574.
- (2011) The composite Archaean grey gneisses: petrological significance, and evidence for a non-unique tectonic setting for Archaean crustal growth. *Lithos*, 123, 21–36.
- Moyen, J.F., and Martin, H. (2012) Forty years of TTG research. *Lithos*, 148, 312–336.
- Neave, D.A., Namur, O., Shorttle, O., and Holtz, F. (2019) Magmatic evolution biases basaltic records of mantle chemistry towards melts from recycled sources. *Earth and Planetary Science Letters*, 520, 199–211.
- Palin, R.M., White, R.W., and Green, E.C.R. (2016) Partial melting of metabasic rocks and the generation of tonalitic–trondhjemitic–granodioritic (TTG) crust in the Archaean: Constraints from phase equilibrium modelling. *Precambrian Research*, 287, 73–90.
- Palin, R.M., Reuber, G.S., White, R.W., Kaus, B.J., and Weller, O.M. (2017) Subduction metamorphism in the Himalayan ultrahigh-pressure Tso Moriri massif: an integrated geodynamic and petrological modelling approach. *Earth and Planetary Science Letters*, 467, 108–119.
- Pamukcu, A.S., Gualda, G.A., Ghiorsio, M.S., Miller, C.F., and McCracken, R.G. (2015) Phase-equilibrium geobarometers for silicic rocks based on rhyolite-MELTS—Part 3: Application to the Peach Spring Tuff (Arizona-California-Nevada, U.S.A.). *Contributions to Mineralogy and Petrology*, 169, 33.
- Pan, R., Macris, C.A., and Menold, C.A. (2020) Thermodynamic modeling of high-grade metabasites: a case study using the Tso Moriri UHP eclogite. *Contributions to Mineralogy and Petrology*, 175, 1–28.
- Pichavant, M., Weber, C., and Villaras, A. (2019) Effect of anorthite on granite phase relations: Experimental data and models. *Comptes Rendus Geoscience*, 351, 540–550.
- Pitzer, K.S., and Sterner, S.M. (1995) Equations of state valid continuously from zero to extreme pressures with H₂O and CO₂ as examples. *International Journal of Thermophysics*, 16, 511–518.
- Powell, R., and Holland, T.J.B. (1988) An internally consistent dataset with uncertainties and correlations: 3. Applications to geobarometry, worked examples and a computer program. *Journal of Metamorphic Geology*, 6, 173–204.
- (2008) On thermobarometry. *Journal of Metamorphic Geology*, 26, 155–179.
- Powell, R., Holland, T.J.B., and Worley, B.A. (1998) Calculating phase diagrams involving solid solutions via non-linear equations, with examples using THERMOCALC. *Journal of Metamorphic Geology*, 16, 577–588.
- Powell, R., Guiraud, M., and White, R.W. (2005) Truth and beauty in metamorphic phase-equilibria: conjugate variables and phase diagrams. *Canadian Mineralogist*, 43, 21–33.
- Robie, R.A., Hemingway, B.S., and Fisher, J.R. (1978) Thermodynamic properties of minerals and related substances at 298.15K and 1 bar (10⁵ pascals) pressure and at higher temperatures. U.S. Geological Survey Bulletin, 1452, 456 pp.
- Sack, R.O., and Ghiorsio, M.S. (1989) Importance of considerations of mixing properties in establishing an internally consistent thermodynamic database: thermochemistry of minerals in the system Mg₂SiO₄-Fe₂SiO₄-SiO₂. *Contributions to Mineralogy and Petrology*, 102, 41–68.
- (1991a) An internally consistent model for the thermodynamic properties of Fe–Mg-titanomagnetite-aluminate spinels. *Contributions to Mineralogy and Petrology*, 106, 474–505.
- (1991b) Chromian spinels as petrogenetic indicators: Thermodynamics and petrological applications. *American Mineralogist*, 76, 827–847.
- (1994) Thermodynamics of multicomponent pyroxenes: I. Formulation of a general model. *Contributions to Mineralogy and Petrology*, 116, 277–286.
- Santos, C.A., Moraes, R., and Szabó, G.A. (2019) A comparison between phase diagram modelling of metamafic rocks and experimental and independent thermobarometric data. *Lithos*, 340–341, 108–123.
- Sen, C., and Dunn, T. (1994) Dehydration melting of a basaltic composition amphibolite at 1.5 and 2.0 GPa: Implications for the origin of adakites. *Contributions to Mineralogy and Petrology*, 117, 394–409.
- Shaw, D.M. (2006) *Trace Elements in Magmas: A Theoretical Treatment*, 256 p. Cambridge University Press.
- Spera, F.J., Bohron, W.A., Till, C.B., and Ghiorsio, M.S. (2007) Partitioning of trace elements among coexisting crystals, melt, and supercritical fluid during isobaric crystallization and melting. *American Mineralogist*, 92, 1881–1898.
- Starr, P.G., Pattison, D.R., and Ames, D.E. (2020) Mineral assemblages and phase equilibria of metabasites from the prehnite–pumpellyite to amphibolite facies, with the Flin Flon Greenstone Belt (Manitoba) as a type example. *Journal of Metamorphic Geology*, 38, 71–102.
- Stuck, T.J., and Diener, J.F. (2018) Mineral equilibria constraints on open-system melting in metamafic compositions. *Journal of Metamorphic Geology*, 36, 255–281.
- Sun, S.S., and McDonough, W.F. (1989) Chemical and isotopic systematics of oceanic basalts: implications for mantle composition and processes. *Geological Society, London, Special Publications*, 42, 313–345.
- Thompson, J.B. (1967) Thermodynamic properties of simple solutions. In P.H. Abelson, Ed., *Researches in Geochemistry*, Vol. 2. Wiley.
- Tomlinson, E.L., and Holland, T.J. (2021) A thermodynamic model for the subsolidus evolution and melting of peridotite. *Journal of Petrology*, 62, egab012.
- White, R.W., and Powell, R. (2002) Melt loss and the preservation of granulite facies mineral assemblages. *Journal of Metamorphic Geology*, 20, 621–632.
- White, R.W., Powell, R., and Holland, T.J.B. (2001) Calculation of partial melting equilibria in the system Na₂O–CaO–K₂O–FeO–MgO–Al₂O₃–SiO₂–H₂O (NCKFMASH). *Journal of Metamorphic Geology*, 19, 139–153.
- (2007) Progress relating to calculation of partial melting equilibria for metapelites. *Journal of Metamorphic Geology*, 25, 511–527.
- White, R.W., Powell, R., Holland, T.J.B., and Worley, B.A. (2000) The effect of TiO₂ and Fe₂O₃ on metapelitic assemblages at greenschist and amphibolite facies conditions: mineral equilibria calculations in the system K₂O–FeO–MgO–Al₂O₃–SiO₂–H₂O–TiO₂–Fe₂O₃. *Journal of Metamorphic Geology*, 18, 497–511.
- White, R.W., Powell, R., and Clarke, G.L. (2002) The interpretation of reaction textures in Fe-rich metapelitic granulites of the Musgrave Block, central Australia: constraints from mineral equilibria calculations in the system K₂O–FeO–MgO–Al₂O₃–SiO₂–H₂O–TiO₂–Fe₂O₃. *Journal of Metamorphic Geology*, 20(1), 41–55.
- White, R.W., Stevens, G., and Johnson, T.E. (2011) Is the crucible reproducible? Reconciling melting experiments with thermodynamic calculations. *Elements*, 7, 241–246.
- White, R.W., Powell, R., Holland, T.J.B., Johnson, T.E., and Green, E.C.R. (2014) New mineral activity–composition relations for thermodynamic calculations in metapelitic systems. *Journal of Metamorphic Geology*, 32, 261–286.
- Whitney, D.L., and Evans, B.W. (2010) Abbreviations for names of rock-forming minerals. *American Mineralogist*, 95, 185–187.
- Whittington, A., Hofmeister, A., and Nabelek, P. (2009) Temperature-dependent thermal diffusivity of the Earth's crust and implications for magmatism. *Nature*, 458, 319–321.
- Yakymchuk, C. (2017) Applying phase equilibria modelling to metamorphic and geological processes: recent developments and future potential. *Geoscience Canada*, 44, 27–45.
- Yakymchuk, C., and Brown, M. (2014) Consequences of open-system melting in tectonics. *Journal of the Geological Society*, 171, 21–40.

MANUSCRIPT RECEIVED JULY 6, 2021

MANUSCRIPT ACCEPTED SEPTEMBER 22, 2021

MANUSCRIPT HANDLED BY ANTONIO ACOSTA-VIGIL

Endnote:

¹Deposit item AM-22-98211, Online Materials. Deposit items are free to all readers and found on the MSA website, via the specific issue's Table of Contents (go to http://www.minsocam.org/MSA/AmMin/TOC/2022/Sep2022_data/Sep2022_data.html).